BULLETIN OF BIOTECHNOLOGY

e-ISSN: 2717-8323

Cilt: 2 Volume: 2 Year: 2021

BULLETIN OF BIOTECHNOLOGY

Cilt: 2 Volume: 2 Year: 2021

Published Biannually

Corresponding Address
Karamanoğlu Mehmetbey University, Faculty of Health, Sciences, Department of Nutrition and Dietetics, Karaman, Turkey
E-mail: mtdogan1@gmail.com
Web: https://www.dergipark.org.tr/biotech

Owner / Publisher
Assist. Prof. Dr. Muhammet DOĞAN
This journal is peer-reviewed and published twice (June, December) a year.

e-ISSN 2717-8323

BULLETIN OF BIOTECHNOLOGY

e-ISSN 2717-8323

Cilt: 2 Volume: 2 Year: 2021

Contents

Research Articles

Tomentosin shows anticancer effect on U87 human glioblastoma multiforme cells 23-26

İlknur ÇINAR AYAN, Ebru GÜÇLÜ, Hatice Gul DURSUN, Hasibe VURAL

The effect of the cross-linker ratio used in gellan gum biomaterial synthesis on biomineralization 27-31

Serbülent TÜRK , Burak ÜNLÜ, Mahmut ÖZACAR

Structural and Thermal Properties of Electrospun Whey Protein/PEO Nanofibers 32-37

Mustafa GÖZLER, Atike İNCE YARDIMCI, Özgür TARHAN

Microwave-assisted Green Biosynthesis of Gold Nanoparticles from Eriobotrya Japonica Leaf Extract 38-43

Gönül SERDAR

5. Biosynthesis of Silver Nanoparticles Using Extract of Fig (Ficus carica) Leaf by Microwave Extraction 44-50

Gönül SERDAR

6. Evaluation of the bioaccessibility of peanut skin polyphenols and their potential use for food enrichment 51-55

Bige İNCEDAYI, Nihal TÜRKMEN EROL

RESEARCH ARTICLE
Bull Biotechnol (2021) 2(2):23-26
https://doi.org/10.51539/biotech.1027492 Jurnal homepage: www.dergipark.org.tr/biotech

Bulletin of Biotechnology

Tomentosin shows anticancer effect on U87 human glioblastoma multiforme cells

İlknur Çınar Ayan[1], Ebru Güçlü[1*], Hatice Gül Dursun[1], Hasibe Vural[1]

[*1]*Department of Medical Biology, Meram Faculty of Medicine, Necmettin Erbakan University, Konya, Türkiye*

*Corresponding author : ebruavc.87@gmail.com
Orcid No: https://orcid.org/0000-0001-5330-6159

Received : 23/11/2021
Accepted : 21/12/2021

Abstract: Glioblastoma multiforme (GBM) is one of the most common brain tumors. Chemotherapy, radiotherapy and surgical resection are methods used in GBM treatment, however, the investigation of possible anticancer effects of low-toxicity natural products on various cancer cells, including GBM, leads to promising results. In this study, it was aimed to investigate anticancer effect of tomentosin, which is a sesquiterpene lactone, on U87 human GBM cells. The cytotoxic effect of tomentosin was evaluated by XTT assay. The concentration of tomentosin that inhibits 50% cell viability (IC_{50}) was determined by the results from XTT, and, in further analyzes cells were treated with tomentosin at IC_{50} concentration. Then, total RNA isolation and cDNA synthesis were performed in control and dose groups, and, the possible anticancer effect of tomentosin was determined by evaluating the expression levels of important genes associated with apoptosis and metastasis by qPCR analysis. In addition, the effect of tomentosin on the colony forming capacity of GBM cells was evaluated by colony formation assay. According to our results, IC_{50} dose of tomentosin was found to be 28.8 µM in U87 cells for 48 hours. When compared to the control group, tomentosin increased expression of *BAX*, *CASP3*, *CASP8*, *CASP9*, *CYCS*, *FADD*, *TNF*, *TNFR1*, *TNFR2* and *TIMP2* genes. And, tomantosin significantly decreased colony forming capacity of U87 cells. In conclusion, it is thought that tomentosin exerts its anticancer effect by changing the expression levels of genes associated with apoptosis and metastasis in U87 GBM cells.

Keywords: Apoptosis; Glioblastoma multiforme; Metastasis; Tomentosin.

1 Introduction

Glioblastoma multiforme (GBM), which accounts for approximately 48% of all malignant primary brain tumors, is one of the deadliest malignancies with a 5-year survival rate of 5.5% and a median survival rate of 15 months (Choi et al. 2020, Tan et al. 2020). Standard treatment for GBM includes a combination of surgical resection, radiotherapy and temozolomide. However, both drug resistance mechanisms and GBM microenvironment limit the effectiveness of treatment methods (Bagherian et al. 2020, Cha et al. 2020).

In the last two decades, studies with cell culture and animal experiments have revealed that natural products with low toxicity can have an anticancer effect by influencing the development and progression of cancer (Kashyap et al. 2021). The identification of natural products that can cross blood-brain barrier, target oncogenic signaling pathways and increase sensitivity to chemotherapy and radiotherapy is very important for the development of new therapeutic strategies against GBM (Park et al. 2017, Vengoji et al. 2018).

Tomentosin, a natural sesquiterpene lactone with various biological activities such as anti-inflammatory, antibacterial and antifungal, is found in medically important members of Asteraceae family such as *Inula viscosa* (Cafarchia et al. 2001, Park et al. 2014, El Omari et al. 2021). In addition, it has been shown that tomentosin inhibits cell proliferation and has an anticancer effect in various cancers such as hepatocellular carcinoma, osteosarcoma, leukemia and gastric cancer (Lee et al. 2019, Yang et al. 2020, Yang et al. 2021, Yu et al. 2021). In this study, it was aimed to investigate the possible anticancer effect of tomentosin on U87 human GBM cells. For this, while determining the cytotoxic and antiproliferative effects of tomentosin were determined on GBM cells, its effect on expression levels of important genes in apoptosis and metastasis was also evaluated. In addition, the effect of tomentosin on the colony forming capacity of U87 cells was investigated.

2 Materials and Method

2.1 Cell culture

U87 (ATCC® HTB-14™) human GBM cell line was purchased from American Type Culture Collection (ATCC, USA). The cells were cultured in high-glucose DMEM medium containing 10% fetal bovine serum and 1% penicillin–streptomycin at 37 ℃, 95% humidity and 5% CO_2.

2.2 Cytotoxicity assay

The cytotoxic effect of tomentosin on U87 cells was determined by 2,3-bis-(2-methoxy-4-nitro-5-sulfophenyl)-2H-tetrazolium-5-carboxanilide (XTT) analysis. For this, U87 cells (10^4 cells/well) were seeded into 96-well plates. After 24 hours, cells were treated with tomentosin at concentrations of 0, 5, 10, 15, 20, 25, 30, 40, 50, 75 and 100 µM for 24, 48 and 72 hours. At the end of the incubation period, XTT solution (Biological Industries, 20-300-1000) was added to each well and absorbance values were read in a microplate reader (BioTek Epoch) at 450 nm wavelength and 630 nm reference range after 4 hours. The concentration of tomentosin that inhibits 50% cell viability (IC_{50}) was calculated by GraphPad Prism 8.0.2 software using XTT data and in further analyzes cells were treated with tomentosin at IC_{50} concentration.

2.3 RNA isolation, cDNA synthesis and qPCR analysis

In this study, expression levels of *BAX*, *BCL2*, *CASP3*, *CASP7*, *CASP8*, *CASP9*, *CASP10*, *CYCS*, *PPARG*, *FAS*, *FADD*, *TNF*, *TNFR1*, *TNFR2*, *MMP2*, *MMP9*, *TIMP1*, *TIMP2*, *CDH1* and *CDH2* genes were evaluated with qPCR. For this, total RNA isolation was conducted with RiboEx (GeneAll, 301-001) in control and dose groups. cDNA synthesis was performed in accordance with the manufacturer's instructions (Bio-Rad, 170-8891). qPCR was performed with reaction mixes containing 5 µl qPCR MasterMix (BrightGreen 2X qPCR MasterMix – ROX, ABM, MasterMix-R), 5 pMol forward primer, 5 pMol reverse primer, and 2 µl cDNA. The reaction was carried out in a Real-time PCR System (Bio-Rad, CFX Connect) for 40 cycles by applying the protocol consisting of enzyme activation (10 minutes at 95˚C), denaturation (15 seconds at 95˚C) and annealing/extension (60 seconds at 60˚C). Analysis was performed by $2^{-\Delta\Delta CT}$ method using GAPDH reference gene.

2.4 Colony formation assay

Control and dose groups cells were seeded at a density of 2×10^3 cells/well into 6-well plate. Cells were incubated at 37°C for 10 days and medium was changed every 2 days. After incubation, cells were fixed with cold methanol for 10 min and stained with 0.5% crystal violet dye. Analysis was performed after counting the stained colonies.

2.5 Statistical analysis

Statistical analysis was performed using t-tests in GraphPad Prism version 8.0.2. "RT2 Profiler ™ PCR Array Data Analysis" program was used quantitative analysis of gene expression results. All experiments were performed in triplicate and data were expressed as mean ± standard deviation. $P < 0.05$ was considered statistically significant.

3 Results

3.1 Tomentosin inhibits U87 cell proliferation

In order to determine the cytotoxic effect of tomentosin, U87 cells were treated with different concentrations of tomentosin for 24, 48 and 72 hours and XTT analysis was performed. According to the results, tomentosin inhibited U87 cell proliferation in a dose- and time-dependent manner (Fig 1). In addition, IC_{50} dose of tomentosin was found to be 28.8 µM in U87 cells for 48 hours. In subsequent analyses, cells were treated with 28.8 µM tomentosin for 48 hours.

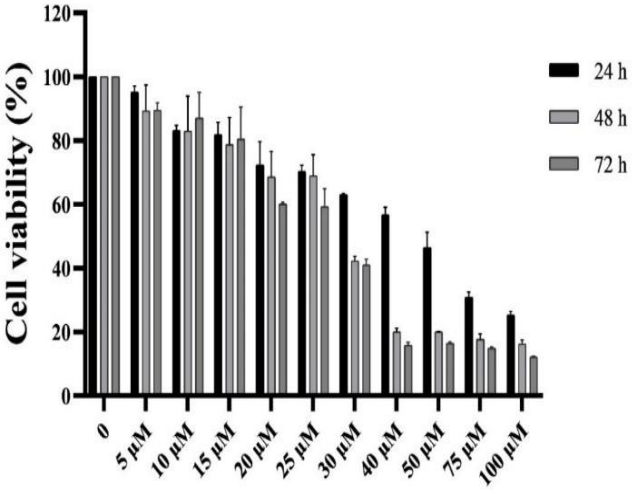

Fig. 1 Effect of tomentosin on U87 cells viability. U87 cells viability (%) was determined by XTT analysis. IC_{50} dose of tomentosin was calculated using XTT data and was found to be 28.8 µM for 48 hours.

3.2 Tomentosin effects expressions of genes associated with apoptosis and metastasis

The effect of tomentosin on expression levels of important genes associated with apoptosis and metastasis was determined by qPCR analysis. Accordingly, expression levels of *BAX*, *BCL2*, *CASP3*, *CASP7*, *CASP8*, *CASP9*, *CASP10*, *CYCS*, *PPARG*, *FAS*, *FADD*, *TNF*, *TNFR1* and *TNFR2* genes associated with apoptosis and *MMP2*, *MMP9*, *TIMP1*, *TIMP2*, *CDH1* and *CDH2* genes associated with metastasis were evaluated in qPCR. After treatment with IC_{50} dose of tomentosin, expression level of *BAX*, *CASP3*, *CASP8*, *CASP9*, *CYCS*, *FADD*, *TNF*, *TNFR1*, *TNFR2* and *TIPM2* genes significantly increased to 2.23, 2.85, 1.75, 1.70, 2.5, 1.52, 3.78, 3.84, 3.81 and 2.12 folds, respectively, compared with control group ($p<0.05$). No significant change was observed in the expression level of *BCL2*, *CASP7*, *CASP10*, *PPARG*, *FAS*, *MMP2*, *MMP9*, *TIMP1*, *CDH1* and *CDH2* genes (Fig 2).

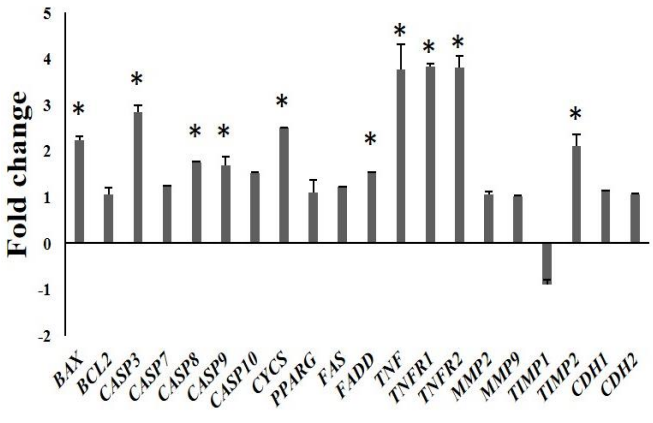

Fig. 2 Effect of tomentosin on expression of important genes in apoptosis and metastasis. *P < 0.05.

3.3 Tomentosin inhibits colony formation of U87 cells

Colony formation assay was performed to determine the effect of tomentosin on growth of U87 cells. Accordingly, tomentosin significantly reduced colony formation of U87 cells (Fig 3).

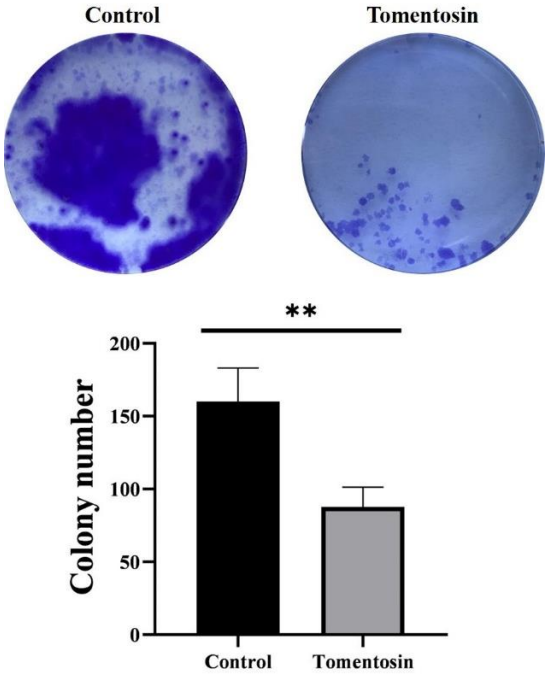

Fig. 3 Effect of tomentosin on colony formation of U87 cells. Cells were treated with IC_{50} dose of tomentosin for 48 hours and cultured for 10 days. **P < 0.01.

4 Discussion

Tomentosin, whose possible anticancer effect on GBM cells was investigated in this study, is a natural sesquiterpene lactone with important biological activities. Sesquiterpene lactones are known to be found in medicinal plants, and it is stated that they cause anticancer effects by changing the redox cell balance and by affecting NF-κB and STAT3, in addition to their various pharmacological properties (Babaei et al. 2018). Studies with various cancer cell lines have also reported the anticancer effect of tomentosin as a sesquiterpene lactone (Merghoub et al. 2017, Lee et al. 2019, Yang et al. 2020, Virdis et al. 2021, Yang et al. 2021, Yu et al. 2021). Virdis et al. (2021) has been shown that tomentosin has an anticancer effect on Burkitt's lymphoma (BL) cells by arresting cell cycle and inducing apoptosis. In addition, researchers stated that tomentosin decreases the expression of anti-apoptotic genes such as *BCL2A1* and *CDKN1A*, increases the expression of *PMAIP1* proapoptotic gene. Similarly, in a study with hepatocellular carcinoma cells, it has been shown that tomentosin induces apoptosis and arrests cell cycle (Yu et al. 2021). And also, it has been stated that tomentosin induces the mitochondria-mediated apoptotic pathway through an increase in the level of reactive oxygen species in leukemia, osteosarcoma, cervical cancer and gastric cancer cells (Merghoub et al. 2017, Lee et al. 2019, Yang et al. 2020, Yang et al. 2021).

In this study, tomentosin inhibited proliferation of U87 human GBM cells. It also increased the expression of genes encoding important proteins involved in the intrinsic and extrinsic pathways of apoptosis (Fulda and Debatin 2006). And, it caused an increase in the expression of *TIMP2*, is effective in the inhibition of MMP2 which provides invasion of cancer cells by destructing of extracellular matrix (Arpino et al. 2015). According to the results of the colony formation analysis, tomenstosin inhibited the U87cell growth and decreased the colony forming capacity of the cells.

5 Conclusion

As a result, it is thought that tomentosin may cause anticancer effects by changing the expression levels of important genes known to play a role in apoptosis and metastasis in U87 human GBM cells. However, further analyzes are required to fully elucidate the anticancer mechanism of tomentosin in GBM.

Acknowledgements

This research did not receive any specific grant from funding agencies in the public, commercial, or not-for-profit sectors.

Authors' contributions: ICA:Investigation, methodology, formal analysis, writing-original draft, writing-review& editing, visualization. EG: Investigation, methodology,formal analysis, writing-original draft, writing-review&editing, visualization. HGD: Investigation, writing-review&editing, supervision. HV: Investigation, writing-review&editing, supervision.

Conflict of interest disclosure: The authors declare that they have no conflict of interest.

References

Arpino V, Brock M, Gill SE (2015) The role of TIMPs in regulation of extracellular matrix proteolysis. Matrix Biol 44-46:247-54.

Babaei G, Aliarab A, Abroon S, Rasmi Y, Aziz SG (2018) Application of sesquiterpene lactone: A new promising way for cancer therapy based on anticancer activity. Biomed Pharmacother 106:239-246.

Bagherian A, Mardani R, Roudi B, Taghizadeh M, Banfshe HR, Ghaderi A, Davoodvandi A, Shamollaghamsari S, Hamblin MR, Mirzaei H (2020) Combination Therapy with Nanomicellar-Curcumin and Temozolomide for In Vitro Therapy of

Glioblastoma Multiforme via Wnt Signaling Pathways. J Mol Neurosci 70(10):1471-1483.

Cafarchia C, De Laurentis N, Milillo MA, Losacco V, Puccini V (2001) Fungistatic activity of a sesquiterpene lactone (tomentosin) isolated from fresh Inula viscosa (Asteraceae) flowers from the Puglia region. Parassitologia 43(3):117-21

Cha GD, Kang T, Baik S, Kim D, Choi SH, Hyeon T, Kim DH (2020) Advances in drug delivery technology for the treatment of glioblastoma multiforme. J Control Release 328:350-367.

Choi J, Kim G, Cho SB, Hyung-Jun I (2020) Radiosensitizing high-Z metal nanoparticles for enhanced radiotherapy of glioblastoma multiforme. J Nanobiotechnol 18, 122.

El Omari N, El Menyiy N, Zengin G, Goh BH, Gallo M, Montesano D, Naviglio D, Bouyahya A (2021) Anticancer and Anti-Inflammatory Effects of Tomentosin: Cellular and Molecular Mechanisms. Separations 8, 207.

Fulda S, Debatin KM (2006) Extrinsic versus intrinsic apoptosis pathways in anticancer chemotherapy. Oncogene 25, 4798–4811.

Kashyap D, Tuli HS, Yerer MB, Sharma A, Sak K, Srivastava S, Pandey A, Garg VK, Sethi G, Bishayee A (2021) Natural product-based nanoformulations for cancer therapy: Opportunities and challenges. Semin Cancer Biol 69:5-23.

Lee CM, Lee J, Nam MJ, Choi YS, Park SH (2019) Tomentosin Displays Anti-Carcinogenic Effect in Human Osteosarcoma MG-63 Cells via the Induction of Intracellular Reactive Oxygen Species. Int J Mol Sci 20(6):1508.

Merghoub N, El Btaouri H, Benbacer L, Gmouh S, Trentesaux C, Brassart B, Attaleb M, Madoulet C, Wenner T, Amzazi S, Morjani H, El Mzibri M (2017) Tomentosin Induces Telomere Shortening and Caspase-Dependant Apoptosis in Cervical Cancer Cells. J Cell Biochem 118(7):1689-1698.

Park HH, Kim SG, Kim MJ, Lee J, Choi BK, Jin MH, Lee E (2014) Suppressive effect of tomentosin on the production of inflammatory mediators in RAW264.7 cells. Biol Pharm Bull 37(7):1177-83.

Park MN, Song HS, Kim M, Lee MJ, Cho W, Lee HJ, Hwang CH, Kim S, Hwang Y, Kang B, Kim B (2017) Review of Natural Product-Derived Compounds as Potent Antiglioblastoma Drugs. Biomed Res Int 2017:8139848.

Tan AC, Ashley DM, López GY, Malinzak M, Friedman HS, Khasraw M (2020) Management of glioblastoma: State of the art and future directions. CA Cancer J Clin 70(4):299-312.

Vengoji R, Macha MA, Batra SK, Shonka NA (2018) Natural products: a hope for glioblastoma patients. Oncotarget 9: 22194-22219.

Virdis P, Marchesi I, Fiorentino FP, Migheli R, Sanna L, Bordoni V, Pintore G, Galleri G, Muroni MR, Bagella L, Fozza C, De Miglio MR, Podda L (2021) Tomentosin a Sesquiterpene Lactone Induces Antiproliferative and Proapoptotic Effects in Human Burkitt Lymphoma by Deregulation of Anti- and Pro-Apoptotic Genes. Life 11(11):1128.

Yang H, Zhao H, Dong X, Yang Z, Chang W (2020) Tomentosin induces apoptotic pathway by blocking inflammatory mediators via modulation of cell proteins in AGS gastric cancer cell line. J Biochem Mol Toxicol 34(8):e22501.

Yang L, Xie J, Almoallim HS, Alharbi SA, Chen Y (2021) Tomentosin inhibits cell proliferation and induces apoptosis in MOLT-4 leukemia cancer cells through the inhibition of mTOR/PI3K/Akt signaling pathway. J Biochem Mol Toxicol 35(4):e22719.

Yu SH, Lee CM, Ha SH, Lee J, Jang KY, Park SH (2021) Induction of cell cycle arrest and apoptosis by tomentosin in hepatocellular carcinoma HepG2 and Huh7 cells. Hum Exp Toxicol 40(2):231-244.

RESEARCH ARTICLE
Bull Biotechnol (2021) 2(2):27-31
https://doi.org/10.51539/biotech.1033344 Jurnal homepage: www.dergipark.org.tr/biotech

Bulletin of Biotechnology

The effect of the cross-linker ratio used in gellan gum biomaterial synthesis on biomineralization

Serbülent Türk[1,2,*], Burak Ünlü[1,2], Mahmut Özacar[2,3]

[*1]*Sakarya University, Biomedical, Magnetic and Semiconductor Materials Application and Research Center (BIMAS-RC), Sakarya University, Sakarya, Turkey*
[2]*Sakarya University, Biomaterials, Energy, Photocatalysis, Enzyme Technology, Nano & Advanced Materials, Additive Manufacturing, Environmental Applications and Sustainability Research & Development Group (BIOENAMS R & D Group), Sakarya University, Sakarya, Turkey*
[3] *Sakarya University, Faculty of Science & Arts, Department of Chemistry, Sakarya, Turkey*

*Corresponding author : serbulentturk@sakarya.edu.tr
Orcid No: https://orcid.org/ 0000-0003-4284-5397

Received : 08/12/2021
Accepted : 24/12/2021

Abstract: The first step in using polymeric materials for many applications is their crosslinking. The crosslinker used in crosslinking before application should be kept at an optimum ratio. The use of gellan gum (GG), a polymeric material, as an intra-body biomaterial is also among these application areas. In this study, the effect of the $CaCl_2$ ratio, used as GG crosslinker, was investigated on the biomineralization of GG hydrogel, which was successfully obtained from 2.5% (w/v) solutions. $GG_{0.5}$, $GG_{1.0}$, and $GG_{1.5}$ hydrogels obtained by crosslinking at 0.5, 1.0, and 1.5% were frozen at −20 °C for 12 h lyophilized at −50 °C at 15Pa for 2 days. FTIR, XRD, SEM, and EDS analyzes of cross-linked GG samples at different rates were performed before and after the biomineralization experiment, for which they were kept in a pre-prepared simulated body fluid medium for 7 days. As a result of the analysis, it was observed that the $GG_{1.0}$ sample, which has a homogeneous surface morphology, has higher P and Ca content and higher bioactivity than the $GG_{0.5}$ and $GG_{1.5}$ samples.

Keywords: Crosslinking; polymer; bioactivity.

1 Introduction

Hydrogels have been extensively studied in tissue engineering and continue to be investigated (Qian at al. 2022). Hydrogel systems consist of cross-linked polymers that can swell when placed in an aqueous medium and, thanks to this swelling feature, are also suitable for drug loading by filling the place where they are implanted. Hydrogels have an advantage over other biomaterials because they have porous structures similar to the extracellular matrix (Akther at al. 2020). In addition, due to their good biocompatibility, they can also be used as carrier materials for cells or bone growth to promote growth factors in bone tissue engineering. Hydrogels attract attention in the field of biomaterials because of their soft tissue adaptability to many soft tissues and their ability to reduce the inflammatory response of surrounding cells and tissues (Bendtsen and Wei, 2015; Tang et al. 2020). Gellan gum, a structure that can be classified as hydrogel, attracts increasing attention in the biomedical field thanks to its versatility and is recommended for tissue engineering applications (Costa et al. 2018; Omar et al. 2021).

Chemical crosslinking agents such as aldehydes, carbodiimides, epoxy and diisocyanates have been widely used in chemical preparation methods. However, most of these agents are toxic to humans. EDC and NHS (Hua et al. 2016), which are other generally used cross-linkers, can also pose a risk of cytotoxicity when used above certain concentrations. It can be used to adjust the elastic modulus of GG hydrogels obtained with crosslinking agents to that which is comparable to that of various human soft tissues such as cartilage. It is also known that the degradation rate is also affected by crosslinking (Choi et al. 2016; Maiti et al. 2021; Ye et al. 2018).

One of the important criteria in biomaterials developed for use in bone tissue engineering is bioactivity (Xue et al. 2018). Bioactivity experiments, in which the formation of bone

structure is examined before in vivo experiments, can be evaluated with in vitro tests (Kokubo and Takadama, 2006). For this, the method of immersion in simulated body fluid (SBF) is generally applied (Bano et al. 2021). Since polymeric hydrogels have certain limitations in the treatment of bone defects due to their poor bioactivity (Lin et al. 2021), these properties of polymeric hydrogels prepared as biomaterials need to be improved.

Although hydrogels have been widely studied for their physical and chemical stability, the bioactivities of these materials need to be improved. In this study, GG hydrogel samples with different crosslinker ratios were prepared. The obtained hydrogel samples were subjected to the bioactivity test. To the best of our knowledge, no study investigating the effect of cross-linking on bioactivity has been found so far.

2 Materials and Methods

Gellan gum (GG) and calcium chloride ($CaCl_2$), were purchased from Sigma Aldrich. Pure water obtained with Millipore Milli-Q was used throughout the study.

GG was dissolved in 2.5% (w/v) deionized water under constant stirring for 15 minutes at 85 °C. To prepare $GG_{0.5}$, $GG_{1.0}$ and $GG_{1.5}$ hydrogels, it is prepared by mixing with the ionic source of $CaCl_2$ at 85°C for 15 min, when used at a rate of 0.5, 1.0 and 1.5%, to be reduced at different rates. The prepared solutions were cooled to room temperature to obtain three-dimensional $GG_{0.5}$, $GG_{1.0}$ and $GG_{1.5}$ hydrogels. Before lyophilization, the hydrogels were frozen at −20 °C for 12 hours. Then, hydrogels were lyophilized at −50°C at 15Pa for 2 days (BIOBASE) after being kept in the pre-prepared SBF (Kokubo and Takadama, 2006) treatment for 7 days in sealed bottles.

Hydrogel samples were analyzed using FTIR (Spectrum Two Perkin-Elmer Co.) by scanning at 4 cm^{-1} resolution in the wavelength range of 4000 cm^{-1}-400 cm^{-1}. Morphological studies were observed using scanning electron microscopy (SEM, JEOL, JMS 6060). The hydrogels, which were previously lyophilized and cut into suitable pieces, were fixed on conductive carbon bands and then covered with a thin layer of gold to ensure conductivity (Polaron CS7620). The elemental distribution in the hydrogels obtained by energy dispersive X-ray spectroscopy (EDS) analysis was analyzed. For the phase characterization of the synthesized hydrogels, analysis was carried out between 5° and 90° using Cu Ka radiation (λ= 0.15406 nm) operating at 40 kV, 30 mA and X-ray diffractometry (XRD, D/Max 2200 LV).

3 Results and Discussion

SEM images of the hydrogel samples incubated for 7 d in SBF are shown in Fig. 1. It was observed that the apatite phase nucleated in the $GG_{1.5}$ sample was larger and less homogeneous compared to the other samples. In the $GG_{0.5}$ and $GG_{1.0}$ samples, a biomineralization process was observed in which homogeneity was preserved. Here, it is predicted that GG chains, which are more compact with the crosslinker effect, are less suitable for apatite nucleation compared to those with less crosslinker ratio. For this reason, it is thought that increasing the crosslinker ratio after a certain rate will affect the homogeneity of the natural bone to be formed in the body.

Elemental composition of $GG_{0.5}$, $GG_{1.0}$, and $OGG_{1.5}$ samples after incubation in SBF was analysed using EDS as shown in Table 1. The amounts of Ca and P elements resulting from CaP formation differ in hydrogel samples obtained by using different crosslinkers. Compared to the GG_1 hydrogel, a higher CaP accumulation was observed on the surfaces of the $GG_{1.0}$ and $GG_{1.5}$ hydrogel samples. Considering the SEM analyzes, due to the homogeneity on the $GG_{1.5}$ surface and the low formation on the $GG_{0.5}$ surface, the subsequent analyzes continued on $GG_{1.0}$, which was chosen as the optimum sample. $GG_{1.0}$ samples before and after immersion in SBF were named as "after GG" and "before GG" in the continuation of the study.

The phase composition was also confirmed by the FTIR. The FTIR spectra of before GG and after GG hydrogels are shown in Fig. 2. For the FTIR spectrum of before GG, the broad band at 3500−3000 cm^{-1} was contributed to stretching vibration of OH^- groups, the characteristic peak at 2925 cm^{-1} was attributed to the stretching vibration of $C–H_2$ groups, the characteristic peaks at 1611 and 1415 cm^{-1} were ascribed to the asymmetric and symmetric stretching vibration of carboxyl groups existed in the salt form, and 1032 cm^{-1} was attributed to the CO– stretching. It has been observed that the results are compatible with the literature (Mohd et al. 2020). Analysis of FTIR spectra of the sample incubated for 7 d in SBF confirms the presence of mineral deposits. Bands indicative for symmetric υ_1 and asymmetric stretching of the phosphate group in the regions 900–1150 cm^{-1}, and asymmetric bending of the PO_4^{3-} group in the region 500–650 cm^{-1}, were observed in after GG hydrogel sample. These peaks, which indicate biomineralization, were similarly observed in previous studies (Aneta et al. 2020; Huijie et al. 2020). This further demonstrated the analytical result of XRD.

Fig. 3 displays the X-ray diffraction pattern of after GG and before GG. GG showed a broad peak at approximately 2θ = 20°, indicated their amorphous nature with lower crystallinity. On comparing the XRD spectra of before GG and after GG, The diffractogram of before GG is typical of amorphous materials with no sharp peaks while diffractogram of after GG shows the sharp crystalline peaks (due to the nucleation of bioapatite) as shown by the presence of peaks at values of 26°, 32°, 33°, 34°, 40°, 46.5° and 49.5° 2θ, which correspond to the (002), (211), (300), (202), (310), (222) and (213) planes of bioapatite, respectively. Similar results for the same phase are also available in the literature (Hossein et al. 2022).

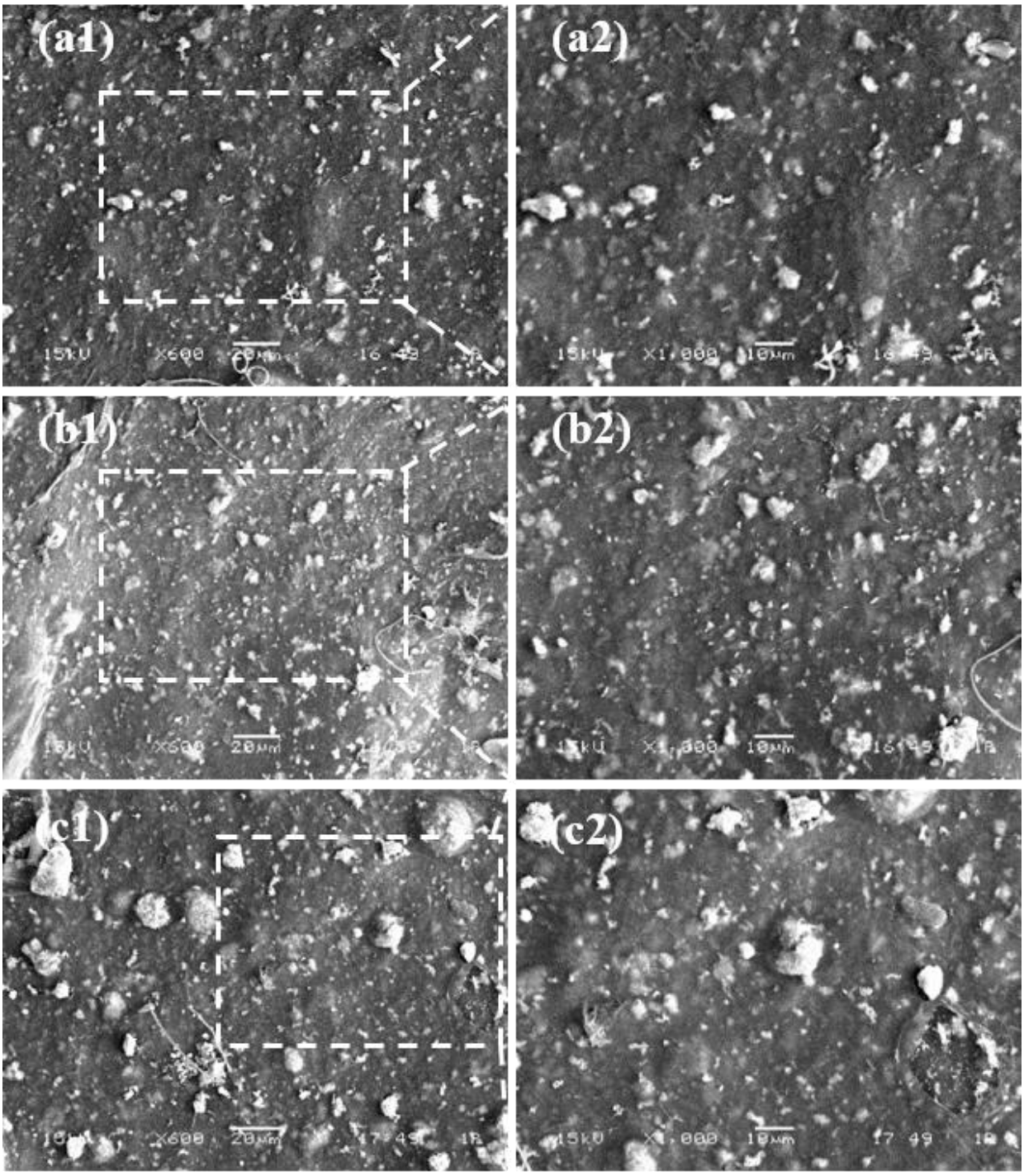

Figure 1. SEM images of (a1, a2) $GG_{0.5}$, (b1, b2) $GG_{1.0}$ and (c1, c2) $GG_{1.5}$ hydrogels.

Table 1. EDS determination of elemental C, O, P, and Ca atomic percentages in lyophilized hydrogels containing different cross linker ratio.

Hydrogel	C	O	P	Ca	Ca/P
	At. (%)				
$GG_{0.5}$	39.56	53.67	2.51	4.26	1.697
$GG_{1.0}$	39.07	51.79	3.41	5.73	1.680
$GG_{1.5}$	39.01	52.27	3.25	5.47	1.683

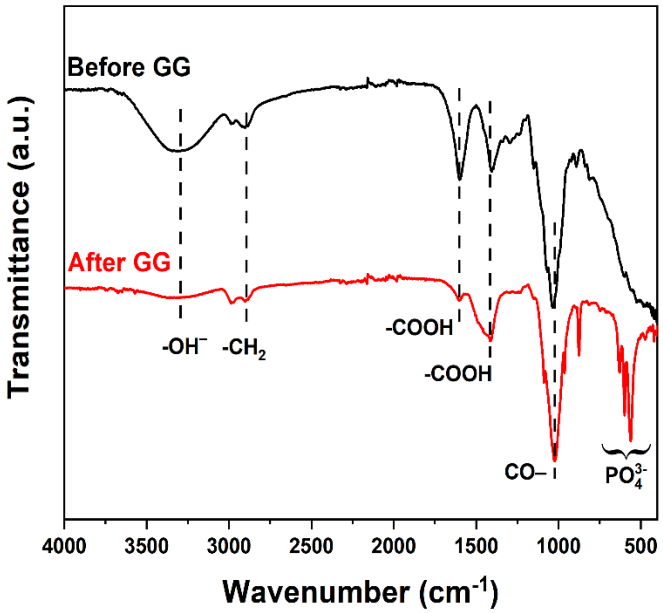

Figure 2. FTIR spectra of before GG and after GG hydrogel samples.

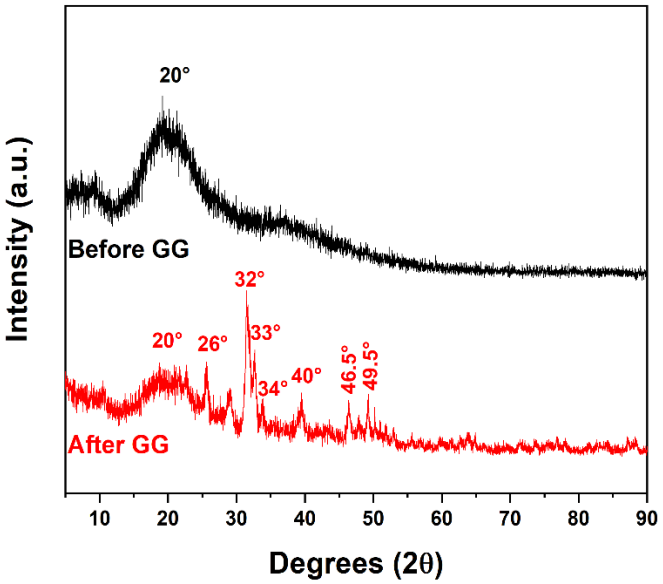

Figure 3. XRD pattern of the (a) before GG, and (b) after GG hydrogels.

4 Conclusion

In this study, hydrogel samples containing different ratios of crosslinker were prepared. In order to examine the bioactivation of the prepared hydrogels, they were kept in SBF for 7 days. Then, drying the hydrogels by lyophilization, the effects of crosslinker on activation were investigated. As a result of these examinations, it was observed that the crosslinker ratio of GG hydrogel affected the bioactivation. It has been found that the crosslinker ratios of GG based hydrogels, which can be used as biomaterials, should be determined before in-vivo studies, and this may contribute significantly to bioactivation and thus to bone formation.

Acknowledgments
This work was supported by the Scientific Research Projects Commission of Sakarya University (Project number: 2019-6-23-223).

Authors' contributions: The authors contributed equally to the article.

Conflict of interest disclosure: No potential conflict of interest was reported by the authors.

References

Akther F, Little P, Li Z, Nguyen N-T, Ta HT (2020) Hydrogels as artificial matrices for cell seeding in microfluidic devices. RSC Adv 10:43682-43703

Aneta P, Anna K, Marta W, Dorota L, Marta G, Andrzej B, Maria N (2019) Halloysite-alkaline phosphatase system—A potential bioactive component of scaffold for bone tissue engineering. Colloids and Surfaces B: Biointerfaces 173:1-8

Bano S, Rincon AR, Grant DM, Nommeots NA, Scotchford C, Ahmed I, Hussain T (2021) In-vitro cell interaction and apatite forming ability in simulated body fluid of ICIE16 and 13-93 bioactive glass coatings deposited by an emerging suspension high velocity oxy fuel (SHVOF) thermal spray. Surface and Coatings Technology 407:126764

Bendtsen ST, Wei M (2015) Synthesis and characterization of a novel injectable alginate-collagen-hydroxyapatite hydrogel for bone tissue regeneration. J Mater Chem B 3:3081–3090

Choi Y, Kim HJ, Min KS (2016) Effects of proanthocyanidin, a crosslinking agent, on physical and biological properties of collagen hydrogel scaffold. Restor Dent Endod 41:296

Costa L, Silva-correia J, Oliveira JM (2018) Gellan Gum-Based Hydrogels for Osteochondral Repair. In: S R J Oliveira J, Pina S, Reis R (ed), Osteochondral Tissue Engineering. Advances in Experimental Medicine and Biology, vol 1058. Springer, Cham

David O, Obada SA, Osseni HS, Kazeem AS, Ayodeji NO, David DA, Naresh DB, Stefan C, Abdulazeez YA, Opeoluwa OF, Adetunji RS, Laminu SK, Muhammad D, Johnson KA, Emmanuel TD (2021) Fabrication of novel kaolin-reinforced hydroxyapatite scaffolds with robust compressive strengths for bone regeneration. Applied Clay Science 215:0169-1317

Hossein K, Mohammad AP, Ali HM, Bahram P, Rouholah A (2022) Facile solution-based synthesis of impurity-free hydroxyapatite nanocrystals at ambient conditions. Journal of Materials Research and Technology 16:656-674

Hua J, Li Z, Xia W, Yang N, Gong J, Zhang J, Qiao C (2016) Preparation and properties of EDC/NHS mediated crosslinking poly (gamma-glutamic acid)/epsilon-polylysine hydrogels. Mater Sci Eng C 61:879–892

Huijie Z, Renchuan Y, Kun Y, Zhentan L, Qunmei F, Xiufang L, Dong W (2020) Silk as templates for hydroxyapatite biomineralization: A comparative study of Bombyx mori and Antheraea pernyi silkworm silks. International Journal of Biological Macromolecules 164:2842-2850

Kokubo T, Takadama H (2006) How useful is SBF in predicting in vivo bone bioactivity? Biomaterials 27:2907–2915

Lin H, Yin C, Mo A, Hong G (2021) Applications of Hydrogel with Special Physical Properties in Bone and Cartilage Regeneration. Materials 14: 235

Maiti S, Khillar PS, Mishra D, Nambiraj NA, Jaiswal AK (2021) Physical and self – crosslinking mechanism and characterization of chitosan-gelatin-oxidized guar gum hydrogel. Polym Test 97:107155

Mohd HR, Nur AI, Khairul AM (2020) Titanium dioxide nanotubes incorporated gellan gum bio-nanocomposite film for wound healing: Effect of TiO_2 nanotubes concentration, International Journal of Biological Macromolecules, Volume 153:1117-1135

Omar A, Lucilia PS, David C, Ricardo A, Subhas CK, Vitor MC, Rui LR (2021) Micropatterned gellan gum-based hydrogels tailored with laminin-derived peptides for skeletal muscle tissue engineering. Biomaterials 279:121217

Tang G, Tan Z, Zeng W, Wang X, Shi C, Liu Y, He H, Chen R, Ye X (2020) Recent Advances of Chitosan-Based Injectable Hydrogels for Bone and Dental Tissue Regeneration. Front Bioeng Biotechnol 8:1–15

Ye B, Zhang S, Li R, Li L, Lu L, Zhou C (2018) An in-situ formable and fi brils-reinforced polysaccharide composite hydrogel by self-crosslinking with dual healing ability. Compos Sci Technol 156:238–246

Qian Y, Jinrong P, Haitao X, Xuewen X, Zhiyong Q (2022) Polysaccharide hydrogels: Functionalization, construction and served as scaffold for tissue engineering. Carbohydrate Polymers 278:118952

Xue J, Feng C, Xia L, Zhai D, Ma B, Wang X, Fang B, Chang J, Wu C (2018) Assembly preparation of multilayered biomaterials with high mechanical strength and bone-forming bioactivity. Chem Mater 30:4646–4657

RESEARCH ARTICLE
Bull Biotechnol (2021) 2(2):32-37
https://doi.org/10.51539/biotech.1034044 Jurnal homepage: www.dergipark.org.tr/biotech

Bulletin of Biotechnology

Structural and thermal properties of electrospun whey protein/PEO nanofibers

Mustafa Gözler[1], Atike İnce Yardımcı[2], Özgür Tarhan[1,*]

*Corresponding author : ozguratarhan@gmail.com
Orcid No: https://orcid.org/0000-0001-7084-6253

Received : 08/12/2021
Accepted : 26/12/2021

Abstract: Nano-scale fibers or films obtained by adding natural active agents to natural food proteins are promising materials for packaging purposes. Whey proteins are one of the most popular matrices in application with their cheap and sustainable availability. They have many functional properties and their antimicrobial, antiviral and anticarcinogenic properties are highlighted as well. Enzymatic hydrolysis can increase their functionality such as inducing gelation and revealing bioactive peptides. These features can make whey proteins good candidates for the fabrication of talented fiber structures through electrospinning. Electrospinning technique based on the deposition of fine fibers on a collector surface under electrical forces can be used to form protein nanofibers. The purpose of this research is to produce whey-based protein nanofibers and determine their structural and thermal features by infra-red spectroscopy and thermogravimetric analysis. A high molecular weight polymer, polyethylene oxide (PEO) was used in combination with whey protein concentrate (WPC) to increase spinnability. Besides, enzymatic hydrolysis of WPC enhanced the viscosity of the protein/polymer solution and helped electrospinning ability. Both non-hydrolyzed and hydrolyzed WPC/PEO nanofibers exhibited promising morphological, structural and thermal properties for targeted use in food and biomedical applications. Further research will focus on the application of these protein nanofibers for the packaging of particular foods.

Keywords: electrospinning; nanofiber; whey; protein; PEO

1 Introduction

To meet the nutritional needs of the increasing world population, it is necessary to benefit from the innovations brought by the emerging technologies to food industry. Producing healthy and high quality products and proper storage ensuring the freshness and safety of these products for a long time without deterioration are critical in industrial manufacturing. Food decay occurs rapidly due to microbiological spoilage and chemical degradation. There are various packaging methods to retard spoilage and extend shelf life. In this context, food packaging and storage have great importance in the food industry. Methods such as modified atmosphere packaging (Erdinç and Acar 1996), vacuum packaging (Jin et al. 2003), and smart packaging (Kocaman and Sarımehmetoğlu 2010) have been developed to preserve the freshness of foods by providing longer shelf life. In recent years, nanofiber based packaging materials obtained from polymers/ biopolymers (eg. food proteins) have been investigated for better protection of food materials as well (Topuz and Uyar 2020). Nanofibers can be produced from both natural and synthetic polymers. Animal- and plant-based proteins are among the natural polymers successfully reported with their nanofiber forms for food applications (Ince Yardımcı and Tarhan 2020). Some animal-based proteins used for nanofiber formation are whey proteins, gelatin, albumin, casein and some plant proteins are soy, zein, gliadin (Zhong et al. 2018, Lin et al. 2019, Tomasula et al. 2016, Wang et al. 2013, Deng et al. 2019). In a general application of electrospinning, clasically, soluble protein solutions are loaded to the syringe needle. Then the positive pole of the power supply is connected to the tip of the needle, and the negative pole is connected to the collector surface. The injector pump starts to work and the pumped protein solution accumulates in the form of fibers on the collecting surface under the produced electric field. These nano-scale fibers gather to form nanofiber films to be used for coating/ packaging of foods. Antimicrobial active agents incorpotared in protein solutions to be electrospun resulted in the formation of nanofiber packaging materials possesing antimicrobial property promising for the extension of shelf life of the target foods.

Whey proteins are widely used sustainable sources for developing novel talented matrices including nanofibers. Protein hydrolysis reveals increased viscosity, thus might support spinnability of proteins. Here, the presented study proposed to compare spinnability of unhydrolyzed and hydrolyzed whey proteins, and investigate some properties. Determination of structural and thermal features of the

nanofiber materials are significant for designing specific coating/packaging applications.

This study aimed to investigate the formation of nanofibers from whey protein concentrate (WPC) and hydrolyzed whey protein concentrate (HWPC) blended with polyethylene oxide (PEO). Within the scope of the presented study, morphological, structural and thermal properties of the WPC/PEO and HWPC/PEO nanofibers were investigated through Scanning electron microscopy (SEM), Fourier transform infrared spectrometer (FTIR), and Thermogravimetric analysis (TGA). Microstructure, typical bondings and interactions within the molecular structure, and thermal durability of the given protein nanofibers were helpful in providing insight regarding their applicability to food systems.

2 Materials and Method

2.1 Materials

To synthesize WPC/PEO nanofibers, PEO (MW of 100.000, Sigma-Aldrich, USA), WPC 80 %, meaning percent protein concentration in wt/wt, (Alfasol, Kimbiotek, Turkey) and ultra pure water were used. Alcalase enzyme (2.4 AU-A/g) was kindly supplied by Novozymes A/S (Bagsvaerd, Denmark).

2.2 Preparation of Protein Solutions

To prepare WPC/PEO and hydrolyzed WPC/PEO, three different solutions were prepared as follows. PEO solution was prepared by dissolving 15 wt % PEO in ultra pure water via mechanical stirring for 12 h at room temperature (RT). The 35 wt % WPC was dissolved in ultra pure water by mechanical stirring for 5 h at RT. The 10 wt % WPC dissolved in ultra pure water was hydrolyzed at 50 ^{o}C in a water bath for 12 h by adding 0.025 g alcalase enzyme (pH 6.5). To obtain a homogen WPC/PEO solution, 5 ml of 35 wt % WPC solution and 5 ml of 15 wt % PEO solution were stirred for 30 min at 1000 rpm (RT). To obtain a homogen HWPC/PEO solution, 2 ml of 10 wt % HWPC solution and 8 ml of 15 wt % PEO solution were stirred for 30 min at 1000 rpm (RT).

2.3 Electrospinning and characterization of WPC/PEO and HWPC/PEO nanofibers

The WPC/PEO and HWPC/PEO solutions were filled into a 20 ml syringe (0.80 mm in diameter) connected to a high voltage for electrospinning. For WPC/PEO sample, 21 kV voltage was applied and flow rate of solution was 0.7 µl/h; for HWPC/PEO sample, 15 kV voltage and 0.652 µl/h flow rate was carried out to obtain nanofibers. The kV values used were determined through preliminary studies. The distance between the syringe and collector was kept constant as 15 cm and the fibers were collected on an Aluminium foil for 3 h.

The morphology of WPC/PEO and HWPC/PEO samples were characterized by SEM (LEO 1430 VP) with an acceleration voltage of 20 kV and a secondary-electron detector. For this purpose, the samples were coated with gold and fixed onto metallic stubs with double-sided carbon tape.

FTIR characterizations of WPC/PEO and HWPC/PEO samples were carried out between 400 and 4000 cm^{-1} wavenumbers with Perkin Elmer UATR Spectrum Two FTIR. The resolution was 4 cm^{-1} and the number of scans collected was 128.

Thermal behavior of nanofibers was determined by TGA (Hitachi STA 7300) analysis in the temperature range of 25-600 ^{o}C under nitrogen atmosphere at a heating rate of 10 ^{o}C /min.

3 Results and Discussion

3.1 Microscopy

The morphological properties of the WPC/PEO fibers were examined with SEM images (Fig 1). While pure PEO is a polymer suitable for electrospinning, the addition of natural food grade protein WPC prevented PEO from being drawn effectively (Zhong et al. 2018). SEM images were carefully evaluated to understand how the whey proteins blended with PEO formed nanofiber.

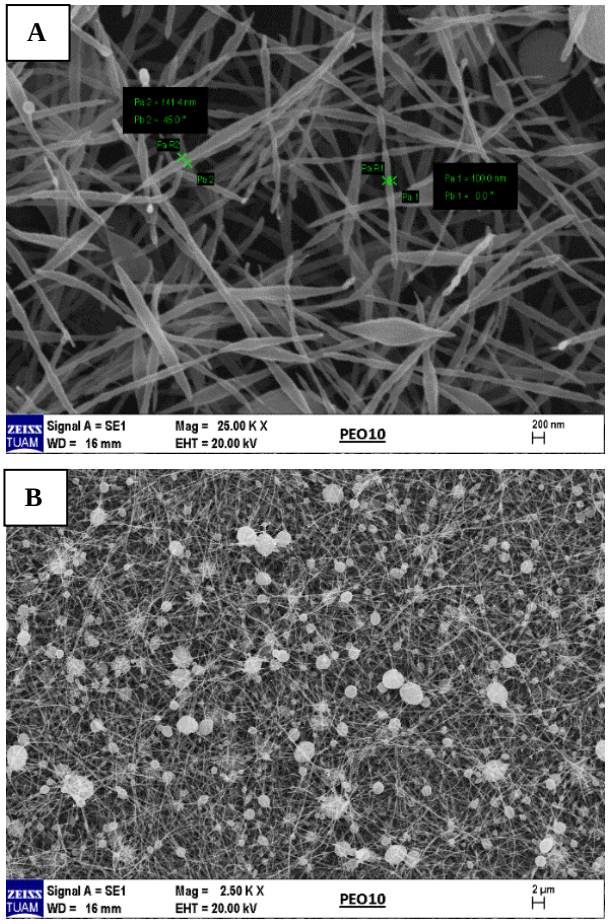

Figure 1. SEM images of WPC/PEO sample with A) high (25.00 KX), and B) low (2.50 KX) magnification

As clearly indicated in Fig 1, fiber formation was achieved in case of WPC/PEO blend. However, beads and short fibers/ breaks were also formed within the nanofiber network. One reason for that is probably the protein concentration in the polymer solution. Equal amount (1:1, v/v) of WPC (35 wt %) and PEO (15 wt %) were mixed and electrospun. This amount of WPC could possibly prevented the formation of regular long fibers to some extend. Besides, addition of higher ratio of WPC in WPC/PEO solution was found to increase bead formation (data not shown). In fact, trails on electrospinning of WPC alone did not result in fiber formation, but PEO alone formed nanofibers in this study (data not shown). Another

reason might be insufficient dissolution of WPC and PEO to be electrospun, thus unhomogenized polymer blend might interrupt the process and caused bead formation and breaks during electrospining. To facilitate electrospinning of WPC and PEO solutions, a better mixing of those should be achieved at higher speeds using an homogenizer. Future work will focus on the optimization of homogenization and electrospinning parameters for WPC/PEO blend. In fact, many factors affect fiber formation, such as electrospinning parameters including flow rate, voltage (Deitzel et al. 2001), distance to the collector (Thompson et al. 2007) and needle diameter (Tan et al. 2005); environmental parameters like temperature, pressure and humidity (De Vrieze et al. 2009; Theron et al. 2004); and solution parameters including polymer molecular weight (Koski et al. 2004), concentration (Deitzel et al. 2001), and electrical conductivity. Therefore, the properties of the solution to be electrospun should be well adjusted to achieve a desirable fiber formation.

SEM images of the HWPC/PEO fibers were given in Fig 2. Although the viscosity of the solution increased (data not shown), bead formation increased as well in case of using hydrolyzed protein instead of unhydrolyzed one. The protein content was lower in hydrolyzed WPC solution (10 wt %) than that of unhydrolyzed one (35 wt %). Thus, under the given conditions hydrolysis causing the formation of smaller protein fragments and aggregates negatively affected spinnability and fiber-forming ability of WPC.

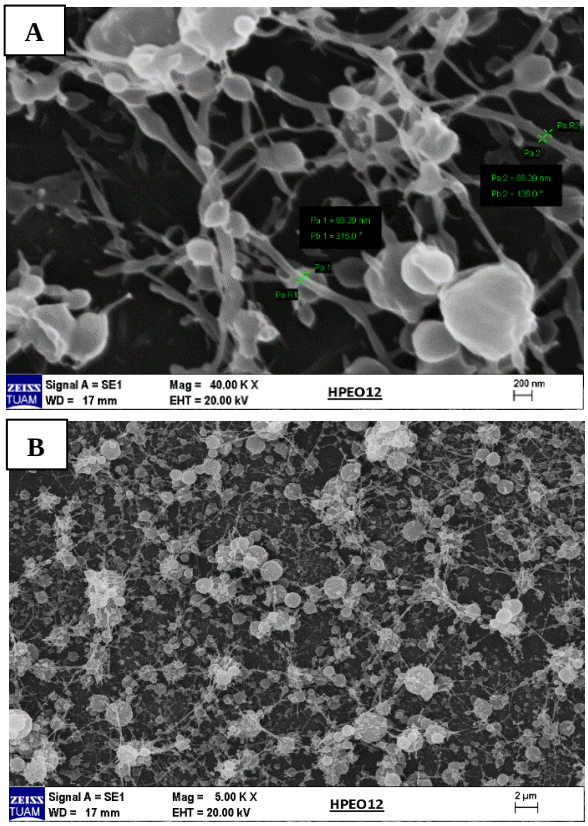

Figure 2. SEM images of the HWPC/PEO sample with A) high (40.00 KX), and B) low (5.00 KX) magnification

3.2. FTIR Analysis

FTIR analysis of protein/polymer nanofibers were given in Figure 3. It is clearly seen that, the peak signal at ~1631 cm^{-1} refers to Amid I stretching vibrations, at ~1541 cm^{-1} attributed to Amide II stretching vibrations (Tarhan et al. 2014). The signals at ~1399 cm^{-1}, 1453 cm^{-1}, ~1242 cm^{-1}, ~1061 and ~1104 cm^{-1} referred to oil, methyl, methylene groups and carbohydrate structures, respectively, in WPC sample (Andrade et al. 2019). Peaks detected at ~699 cm^{-1}, 1467 cm^{-1}, 1360 cm^{-1} and 2884 cm^{-1} indicated the presence of PEO (Ratna et al. 2006).

Similarly, remarkable signals corresponding to Amide I and II vibration modes of the WPC proteins and -CH_2 stretching modes of PEO were detected in HWPC/PEO sample, in agreement with the literature (Ratna et al. 2006, Tarhan and Şen 2022). The peak heights lowered since the amount of intact WPC was lower in the HWPC/PEO sample as a result of protein hydrolysis. The α-helical elements represented by the amide vibrational peaks at the given wavenumbers in unhydrolyzed protein degraded in case of hydrolysis. It was evident with the significantly lowered signals at ~1631 and 1541 cm^{-1} in the latter case. Alterations of the structural conformation of proteins revealed through hydrolysis. In general, helical structures are disturbed through enzyme digestion revealing exposed β-sheet and random coil structures leading to new conformational arrangements within protein structure (Tarhan and Şen 2022).

The presence of WPC in fiber prefixes was evident due to FT-IR findings (Fig3A). Besides, the peaks observed in the spectrum showed the presence of PEO in fiber samples obtained from WPC and PEO polymer blends.

3.3 TGA Analysis

Thermograms of WPC/PEO and HWPC/PEO were presented in Figure 4. The blue line in the graphs indicated the weight loss in WPC/PEO sample, the fracture at 100ºC indicated the evaporation of the water, after 300º C the weight loss of WPC itself were shown (Islam et al. 2014), and the weight loss after 400º C revealed the degredation of PEO (Balo et al. 2019).
The HWPC/PEO sample lost its weight as a result of a single stage decomposition after 400º C. The protein was hydrolyzed through 12 h before electrospinning and thus, the polymer solution contained hydrolysis products instead of intact protein. Nanofibers with beads were formed from peptide fragments of degraded WPC molecules. Different from WPC/PEO graph, there was no peak representing WPC loss in the HWPC/PEO graph and the transition was smooth. This clearly indicated that there was no intact WPC molecule in the nanofiber network.

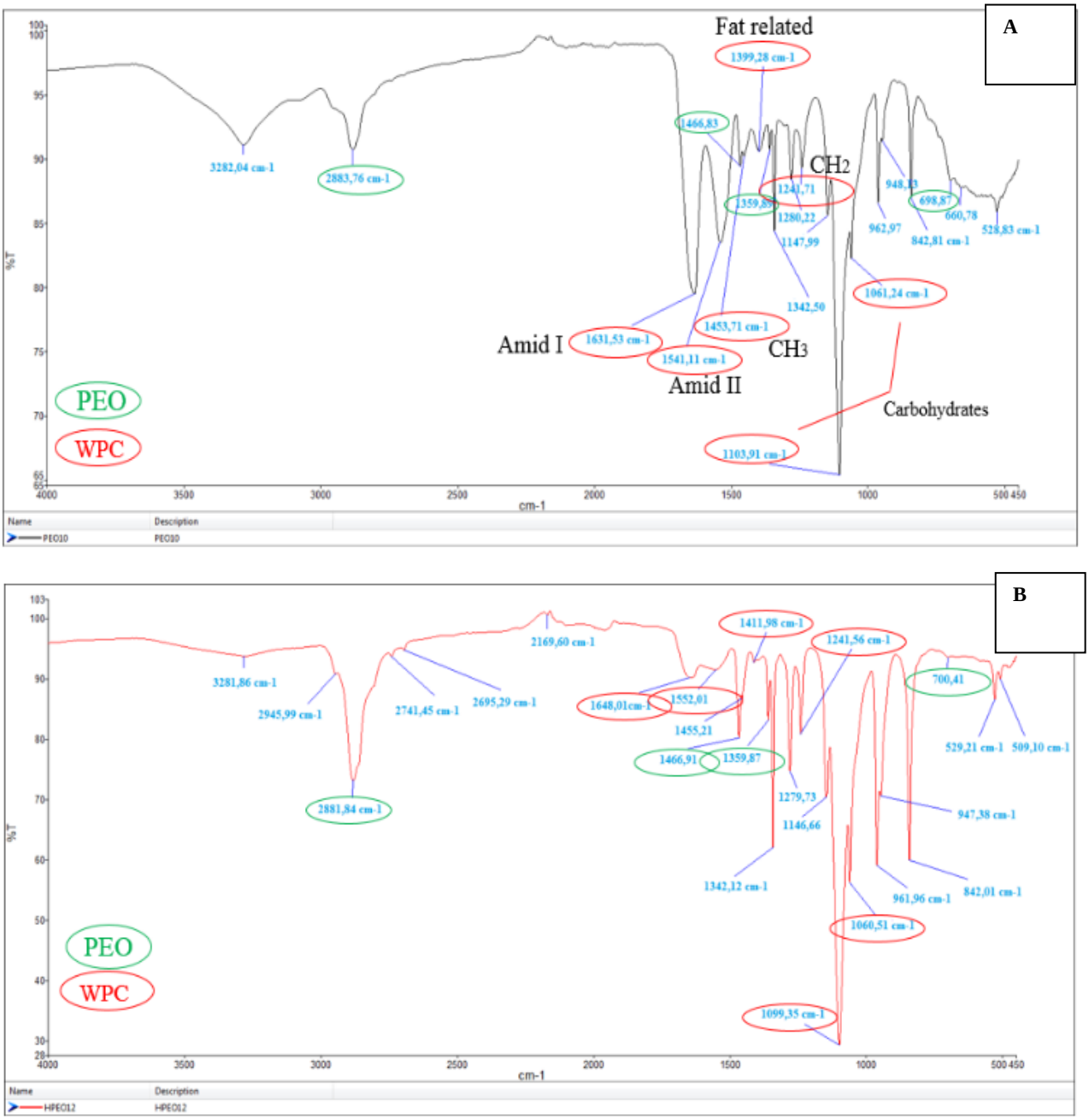

Figure 3. FTIR spectrum of the WPC/PEO (A), HWPC/PEO (B) samples

4. Conclusion

It was observed that WPC, a natural animal-based protein, could form continuous electrospun nanofibers in the presence of the synthetic polymer PEO with a ratio of 1:1 (v/v). Based on the SEM images, the WPC/PEO sample exhibited better spinnability than the HWPC/PEO sample. It was evident that HWPC increased bead formation due to some reasons such as the presence of low molecular weight peptide fragments discouraging spinnability and non-homogeneous mixture of protein/peptide and PEO solution. Thus, better mixing of the electrospinning solutions through the homogenizer will be beneficial for more effective fiber formation. FTIR plots confirmed the presence of WPC, HWPC and PEO in the resultant nanofiber structures. According to TGA findings, thermal degradation of WPC and PEO occurred at 300 ºC and 400 ºC, respectively, and almost all WPC was degraded during hydrolysis. Based on the structural and thermal properties of nanofibers derived from WPC could be considered as proper matrices for different applications. Further research will focus on investigating additional characteristics of WPC/PEO nanofiber materials and their efficiency in food packaging applications.

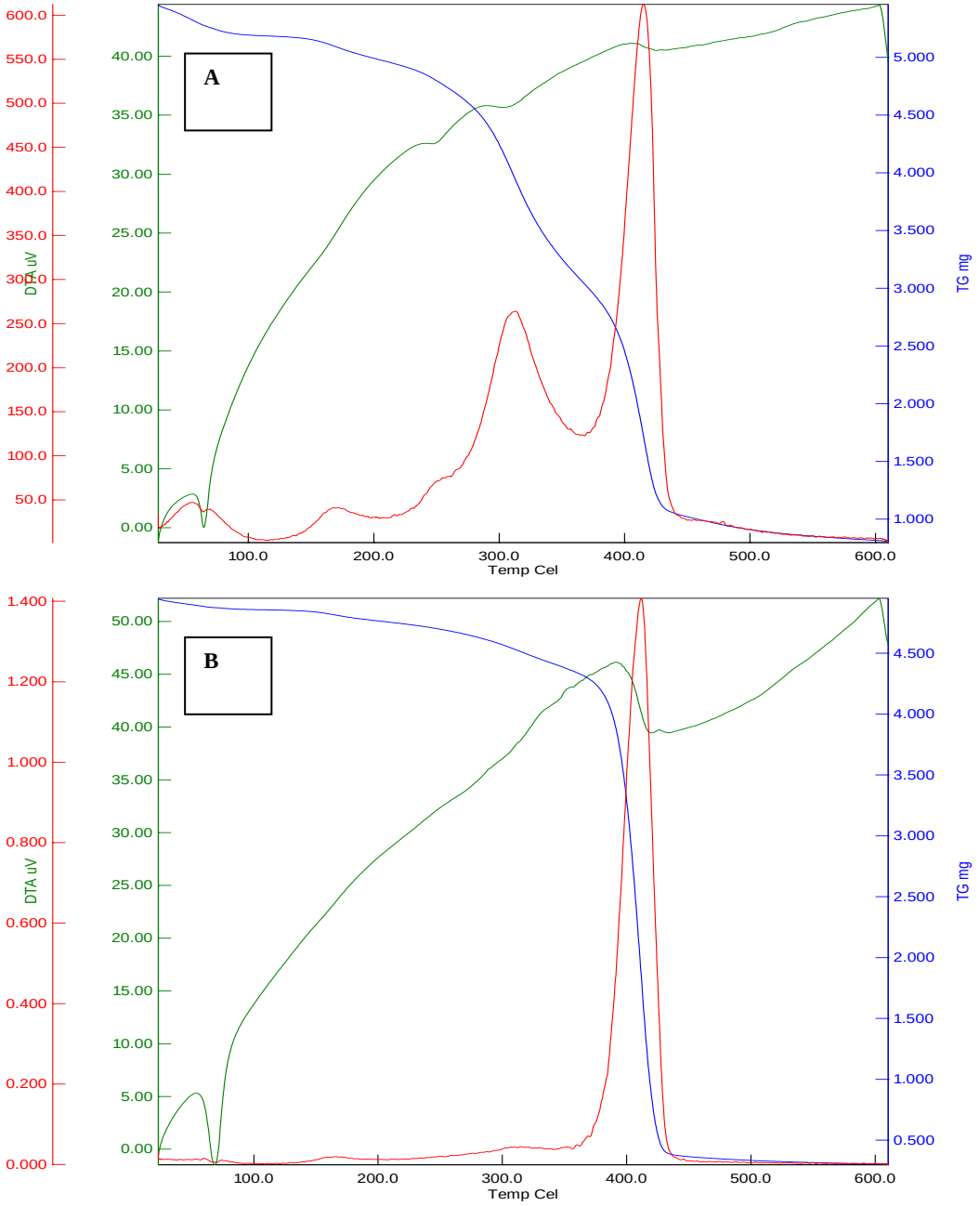

Figure 4. TGA scan of WPC/PEO (A), HWPC/PEO (B) samples

Acknowledgement

The authors are very thankful to Scientific Analysis, Technological Application, and Research Center of Usak University for FT-IR measurements.

References

Andrade J, Pereira CG, de Almeida Junior JC, Viana CCR, de Oliveira Neves LN, da Silva PHF, Bell MJV, dos Anjos VDC (2019) FTIR-ATR determination of protein content to evaluate whey protein concentrate adulteration. LWT-Food Sci and Tech 99: 166-172

Balo L, Gupta H, Singh SK, Singh VK, Tripathi AK, Srivastava N, Tiwari RK, Mishra R, Meghnani D, Singh RK (2019) Development of gel polymer electrolyte based on LiTFSI and EMIMFSI for application in rechargeable lithium metal battery with GO-LFP and NCA cathodes. J of Solid State Electrochemistry 23(8): 2507-2518

Deitzel JM, Kleinmeyer J, Harris DEA, Tan NB (2001) The effect of processing variables on the morphology of electrospun nanolifs and textiles. Polymer 42(1): 261-272

Deng L, Li Y, Feng F, Wu D, Zhang H (2019) Encapsulation of allopurinol by glucose cross-linked gelatin/zein nanofibers: Characterization and release behavior. Food Hydrocolloids 94: 574-584

De Vrieze S, Van Camp T, Nelvig A, Hagström B, Westbroek P, De Clerck K (2009) The effect of temperature and humidity on electrospinning. Journal of Mat Sci 44(5): 1357-1362

Erdinç B, Acar J (1996) Gıda muhafazasında modifiye atmosfer paketleme (MAP). Gıda 21(1): 17-21

Islam MS, Hamdan S, Ahmad MB, Hasan M, Hassan A, Haafiz MM, Jawaid M (2014) Effect of PVA-co-MMA copolymer on the physical, mechanical, and thermal properties of tropical wood materials. Advances in Mat Sci and Eng doi.org/10.1155/2014/626850

İnce Yardımcı A, Tarhan Ö (2020) Electrospun protein nanofibers and their food applications. Mugla J of Sci and Tech 6(2): 52-62

Jin Y, Wang ZF, Lim PC, Pan DY, Wei J, Wong CK (2003) MEMS vacuum packaging technology and applications. In: Proceedings of the 5th electronics packaging technology conference (EPTC 2003), IEEE, Singapore, 10-12 December 2003, pp 301-306

Kocaman N, Sarımehmetoğlu B (2010) Use of smart packaging in foods. Veteriner Hekimler Derneği Dergisi 81(2): 67-72

Koski A, Yim K, Shivkumar S (2004) Effect of molecular weight on fibrous PVA produced by electrospinning. Materials Letters 58(3): 493-497

Lin L, Gu Y, Cui H (2019) Moringa oil/chitosan nanoparticles embedded gelatin nanofibers for food packaging against Listeria monocytogenes and Staphylococcus aureus on cheese. Food Packaging and Shelf Life 19: 86-93

Ratna D, Divekar S, Samui AB, Chakraborty BC, Banthia AK (2006) Poly (ethylene oxide)/clay nanocomposite: thermomechanical properties and morphology. Polymer 47(11): 4068-4074

Tan SH, Inai R, Kotaki M, Ramakrishna S (2005) Systematic parameter study for ultra-fine lif fabrication via electrospinning process. Polymer 46(16): 6128-6134

Tarhan Ö, Tarhan E, Harsa Ş (2014) Investigation of the structure of alpha-lactalbumin protein nanotubes using optical spectroscopy. Journal of Dairy Research 81(1): 98-106

Tarhan Ö, Şen R (2022) Heat-denatured and alcalase-hydrolyzed protein films/coatings containing marjoram essential oil and thyme extract. Food Biosci 45: 101466 doi.org/10.1016/j.fbio.2021.101466

Theron SA, Zussman E, Yarin AL (2004) Experimental investigation of the governing parameters in the electrospinning of polymer solutions. Polymer 45(6): 2017-2030

Thompson CJ, Chase GG, Yarin AL, Reneker DH (2007) Effects of parameters on nanolif diameter determined from electrospinning model. Polymer 48(23): 6913-6922

Tomasula PM, Sousa AM, Liou SC, Li R, Bonnaillie LM, Liu L (2016). Electrospinning of casein/pullulan blends for food-grade applications. J of Dairy Science 99(3): 1837-1845

Topuz F, Uyar T (2019) Antioxidant, antibacterial and antifungal electrospun nanofibers for food packaging applications. International Int Food Res J 130: 108927 doi.org/10.1016/j.foodres.2019.108927

Wang S, Marcone MF, Barbut S, Lim LT (2013) Electrospun soy protein isolate-based fiber fortified with anthocyanin-rich red raspberry (Rubus strigosus) extracts. Food Research Int 52(2): 467-472

Zhong J, Mohan SD, Bell A, Terry A, Mitchell GR, Davis FJ (2018) Electrospinning of food-grade nanofibres from whey protein, Int J Biol Macromol 113: 764-773

RESEARCH ARTICLE
Bull Biotechnol (2021) 2(2):38-43
https://doi.org/10.51539/biotech.1034330 Jurnal homepage: www.dergipark.org.tr/biotech

Bulletin of Biotechnology

Microwave-assisted green biosynthesis of gold nanoparticles from *Eriobotrya japonica* leaf extract

Gönül Serdar*

*Karadeniz Technical Universty, Central Research Laboratory,Trabzon, Turkey.

*Corresponding author : gonulserdar@ktu.edu.tr
Orcid No: https://orcid.org/0000-0002-3589-2323

Received : 08/12/2021
Accepted : 23/12/2021

Abstract: In this study, as industrial waste, prina was used as an adsorbent substance with its natural and thermally modified form. The prina used in the study was taken as waste material from an olive oil factory in Ayvalık, Turkey. In this study, the removal possibilities of the toxic effect of crystal violet dye found in various industrial wastewaters with prina adsorbent were investigated. By using the pyrolysis method at 600 °C, the biochar form of prina was obtained. Natural and biochar prina and crystal violet (CV) dye have been tried under different adsorption conditions. For this purpose, experiments were carried out at different prina dosages, initial dye concentrations and contact times. The highest removal efficiencies are around 75% in natural prina, while the biochar is around 99% in prina. Also, concentration studies were applied to Langmuir and Freundlich adsorption isotherm models. As a result of the isotherm study, it was seen that the adsorption mechanism was suitable for Freundlich isotherm model. The contact time removal studies were applied to pseudo-first-order, pseudo-second-order and intraparticle diffusion kinetic models, and adsorption was found to be fit with the pseudo-second-order kinetic model. According to the experiment results, it was observed that the thermal treatment caused a significant increase in the removal efficiency. It was found that it is an efficient adsorbent material that can be used to remove the CV dye from the aqueous solutions.

Keywords: Adsorption; biochar; crystal violet; dye removal; isotherms; kinetics.

1 Introduction

Erioboytrya japonica (Thunb.), known as loquat, is a multipurpose herb. Its leaves have been used as herbal medicine in the treatment of cough thanks to chemical components such as flavonoids, triterpenoid acid and sesquiterpene glycosides . In this study, aimed to the microwave-assisted green synthesis method to obtain gold nanoparticles from *Eriobotrya Japonica* leaves without using toxic chemicals. For this reason, biomolecules and metabolites are *Erioboytrya japonica* (Thunb.) leaves will be used as reducing and capping agents to prevent agglomeration by stabilizing nanoparticles (Zhao et al. 2015). Therefore, it is needed for the improvement of the environment approach to synthesize metal and metal oxide nanomaterials to make use of for the produced of nanoparticles. Plants (Ryaidh et al. 2017), fungi (Molnár et al. 2018), algae (Kathiraven et al. 2015), bacteria (Deljou and Goudarzi 2021) and yeasts (Niknejad et al. 2015) because they ınclude metabolites that own the ability to reduce metallic salts and formulate nanoparticles. Also, these items they act both as a reducing agent and also take part in the stabilization of nanostructures. It has been accomplished with new nanoparticle practices such as antibacterial activity, cancer therapy, antioxidant activity, drug delivery systems, removal of toxic pollutants from wastewater and catalytic activity (Drummer et al. 2021). The biological synthesis route has some advantages such as renewable, minimal energy, sustainable industrialscale manufacturing, operating costs and negligible toxicity in waste.

Plant extracts appear to be excellent biological media because they more stable, reduce metal ions more rapidly (Singh et al. 2016; Hussain et al. 2016; Kharissova et al. 2013). Primary and secondary metabolites of plants are account in order to the reduction of metallic ions in synthesis (Rastogi et al. 2018). Major phytochemicals contain carbohydrates terpenoids, saponins, phenols, proteins and alkaloids that hoped to induce some shape control while the reduction reaction (Ovais et al. 2018). The size and morphology of nanoparticles affect their optical and electrical properties. Therefore, these features are controlled so as to beter improvement in the subject of “green” nanotechnology such as reaction temperature concentration, contact time, pH factors act the properties of green synthesized nanoparticles

(Drummer et al. 2021). Microwave synthesis has been progressively exerted different subjects of materials and chemicals science (Kumar and Sanghi 2012; Tanan and Saengsuwan, 2014) by means of its usually simple, reaction rate and rapid volumetric heating. When determining a method to synthesize NPs, some factors of producing pure NPs are important such as short reaction times, high the efficiency. the shape and morphology of the formed nanostructures can be checked in this procedure (Parveen et al. 2016: El-naggar et al. 2016).

2 Materials and Method

2.1 Materials

Erioboytrya japonica leaves were collected at the Eastern Black Sea region (Trabzon,Turkey). The leaves were air dried on for several days after washed with distilled water. The dried leaves were ground into powder in a grinder to be stored for use. Hydrogen tetrachloroaurate (III) hydrate ($HAuCl_4.3H_2O$) were obtained from Sigma Aldrich.

2.2 Preparation of gold nanoparticles

20 g of *Erioboytrya japonic*) leaf powder was shaken in 400 mL distilled water for 90 minutes at 25 ºC before being extracted in a laboratory microwave device (Milestone, Start S Microwave, USA) for 4 minutes at 600 W power. After filtration utilizing Whatman No. 1 filter paper, the filtrate was kept at 4 °C for use in the biosynthesis of AuNP experiments. Various volume of leaf extract (3.4.5 mL) was added to 30 mL of $HAuCl_4.3H_2O$ solution (0.5 mM, 1 mM, 2 mM) to synthesize AuNPs. For the synthesis of AuNPs, optimum reaction parameters were determined by exposing the mixture to a household microwave for 1-60 min. at 90W power. The color change from colorless to pale yellow/purple pink obtained by microwave treatment is evidence of colloidal AgNP formation in solution. Analyzes were carried out in three replicates.

2.3 UV–visible spectroscopy

Biosynthesis of AuNPs can be monitored with UV-vis spectroscopy by reducing the gold ion solution using Erioboytrya japonica leaf extract. The formation of the reduced AuNP colloidal solution was followed using UV-vis spectra. Color changes were watched both visually and by absorbance measurements utilizing a spectrophotometer. Spectra of surface plasmon resonances of AuNPs were registered utilizing a UV-vis spectrophotometer at wavelengths in the range 300-800 nm.

3 Results and Discussion

The color change of the solutions from pale yellow to yellowish brown is a sign of nanoparticle formation (Fig.1).

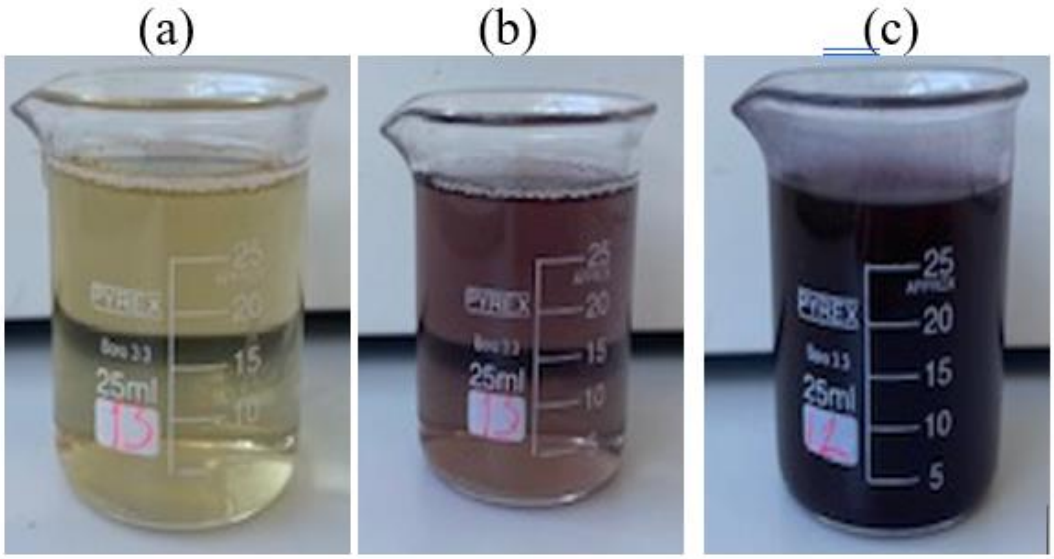

Fig 1. Color change of HAuCl4.3H20 and *Erioboytrya japonica* leaves extract mixture (a) before and (b and c) after microwave treatment.

The UV-visible spectrum of AuNPs is presented in the range 300–800 nm in Fig.(2), Fig.(3), Fig.(4). SPR absorption spectra of silver nanoparticles produced from 0.5 mM, 1 mM, 2 mM $HAuCl_4.3H_2O$ concentration. Spectrophotometric scanning of the mixture of (3,4,5 mL) Erioboytrya japonica leaf extract and (0.5 mM, 1mM, 3 mM) HAuCl4.3H2O solution were performed at different times after microwave treatment. Fig.(2), Fig.(3), Fig.(4) were presented the UV-visible spectrum of AuNPs in the range of 300-800 nm. SPR absorption spectra of silver nanoparticles produced using (0.5 mM, 1 mM, 2 mM) $HAuCl_4.3H_20$ solution are given in below figures.

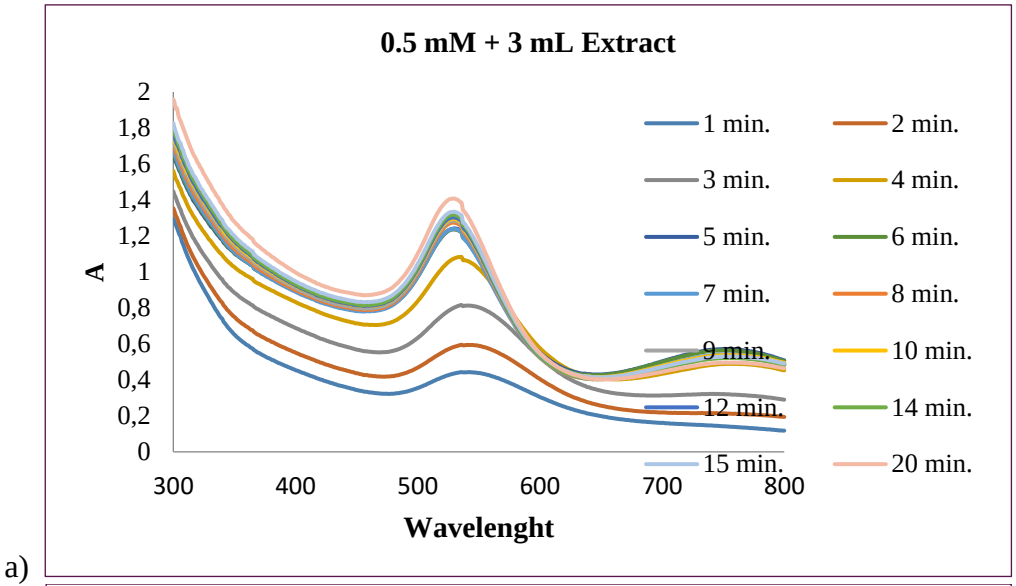

a)

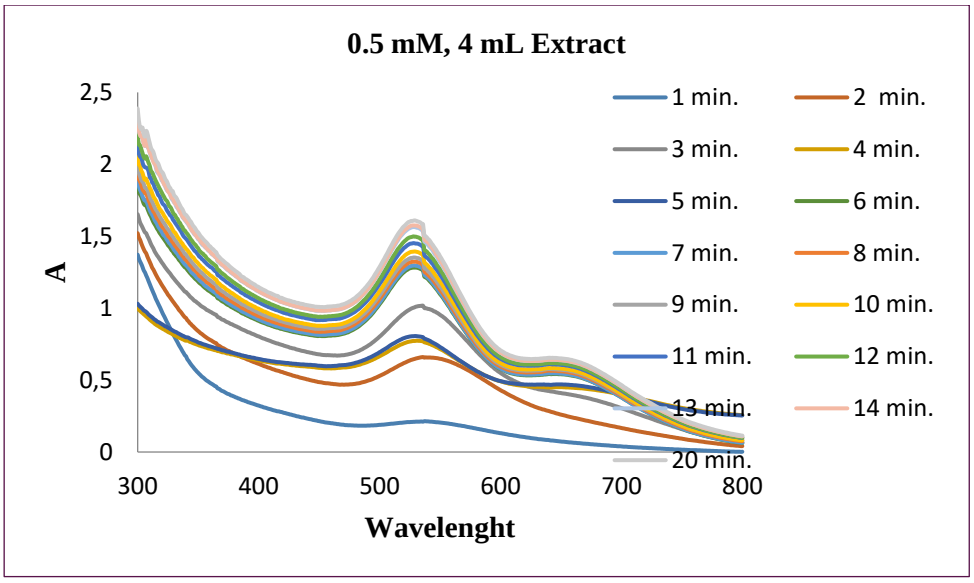

b)

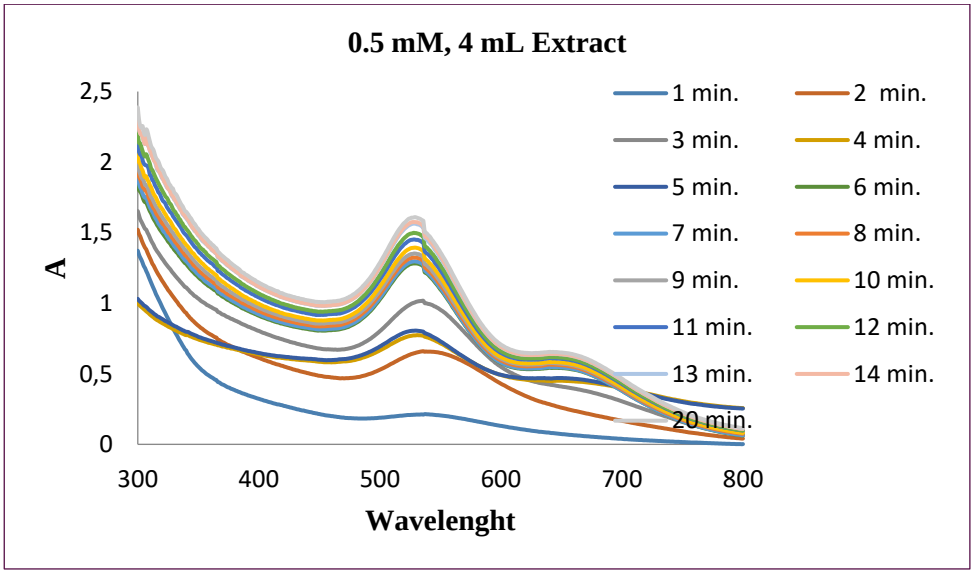

c)

Fig 2. SPR absorption spectra of gold nanoparticles produced from 0.5 mM [a (3 ml), b (4 ml), c (5 ml)] $HAuCl_4.3H_20$ concentration.

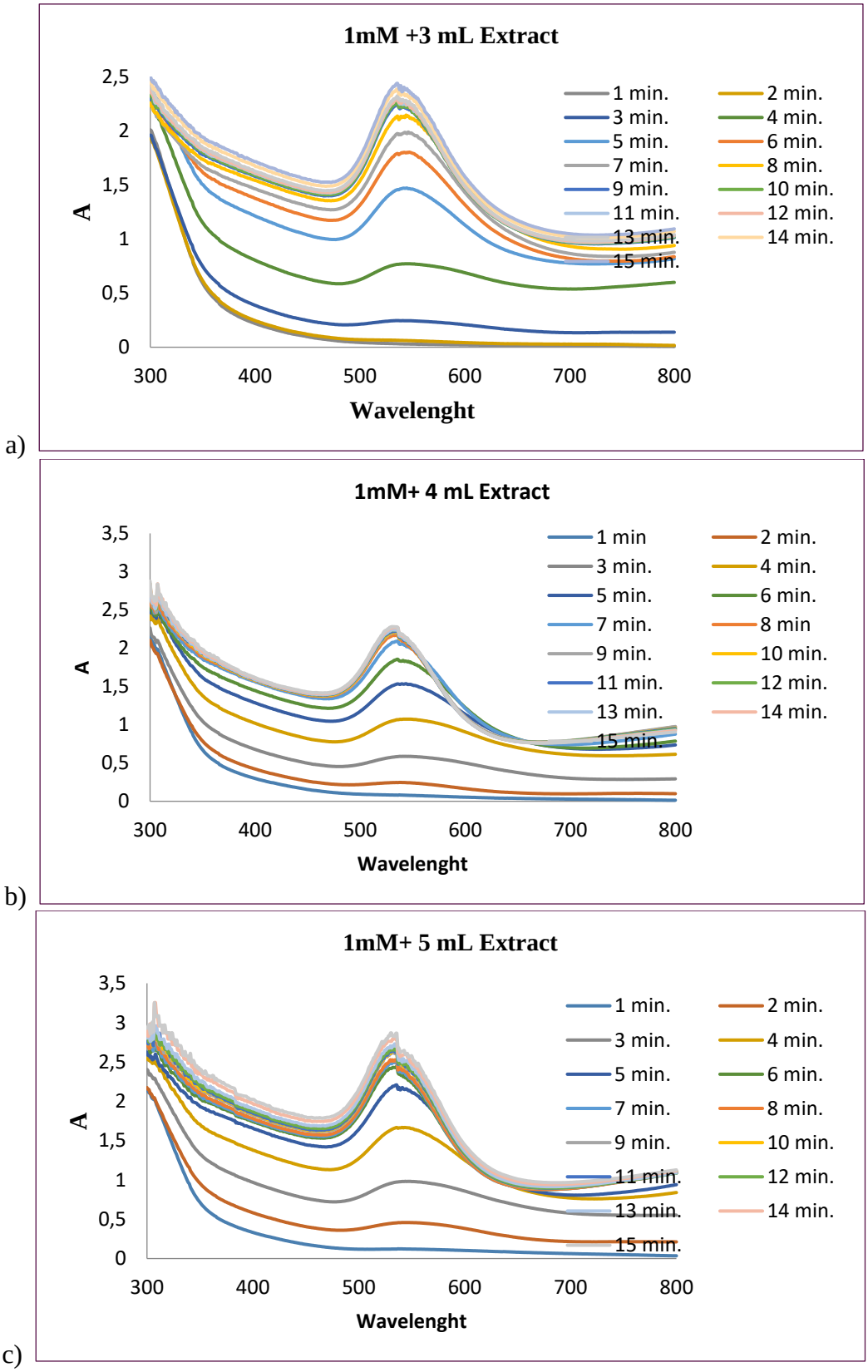

Fig 3. SPR absorption spectra of gold nanoparticles produced from 1 mM [a (3 ml), b (4 ml), c (5 ml)] $HAuCl_4.3H_20$ concentration.

a)

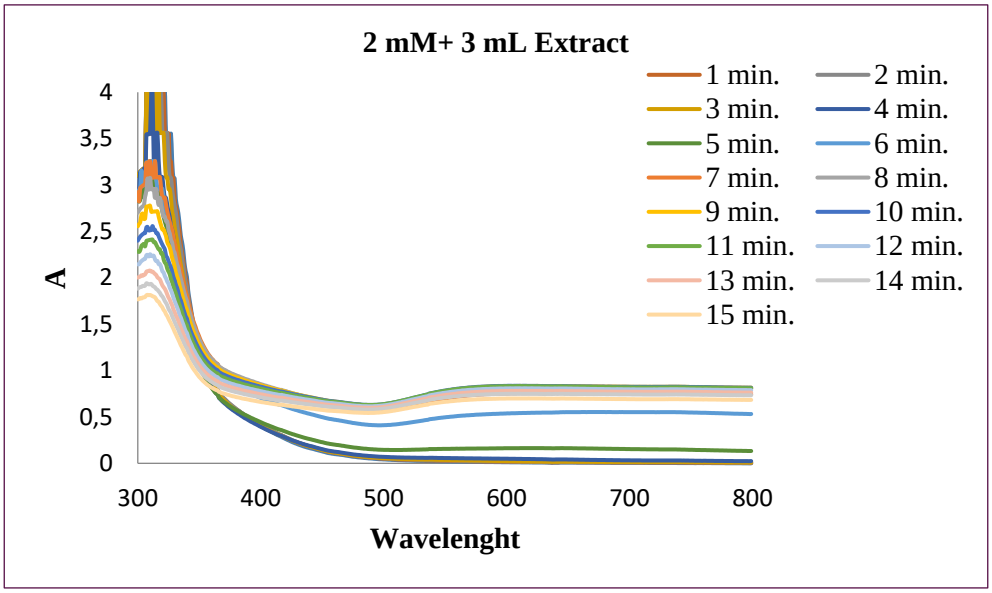

b)

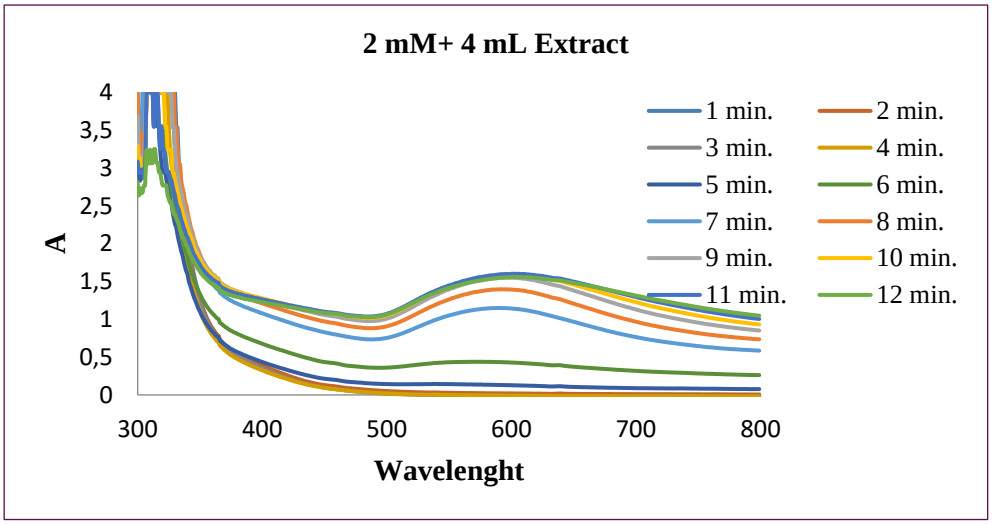

c)

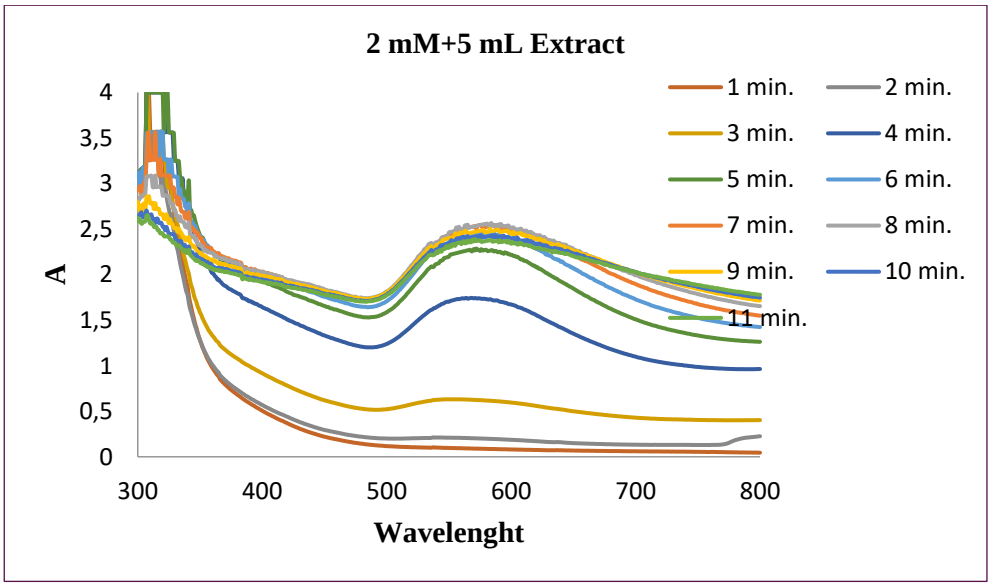

Fig 4. SPR absorption spectra of gold nanoparticles produced from 2 mM [a (3 ml), b (4 ml), c (5 ml)] $HAuCl_4.3H_20$ concentration.

AuNPs were produced as given in Fig.(2), Fig.(3), Fig.(4). By increasing $HAuCl_4.3H_2O$ concentration and keeping other parameters same, obtaining wider resonance bands were showed the formation of larger nanoparticles. SPR absorption spectra was observed 530 and 600 nm region. The specific resonance band was observed after 5 minutes of exposure with 3 mL and 4 mL extracts, while it was observed after 4 minutes with 5 mL of extract. The band reached to maximum height after 7 minutes microwave treatment at 90 W power in Fig (3). The peak intensity and full width at half maximum were affected by the size and degree of agglomeration of particles. Thereby, in all cases the width of the peak can be attributed to the broad particle size distribution (Sökmen et al., 2017).

4 Conclusions

Biomolecules present in extract and microwave treatment facilitates the nanoparticle production are able to reduce gold ions to gold nanoparticles. The color change from light to dark purple color was surveyed throughout the reaction with changing concentration of Erioboytrya japonica leaf extract, which are the SPR of AuNPs in solution. The specific resonance band was observed around 530 - 600 nm region, indicating the formation of AuNPs. It is clear that AuNPs were succesfully produced with 3 mL, 4mL, 5 mL extract and (0.5mM, 1mM) $HAuCI_4.3H_2O$ solution by micowave asisted extraction. Extract concentration has an influence in detecting the size distribution of AuNPs. Produced collaidal solutions were monitored for 40 days. A fast, simple and economical production of AuNP was achieved using *Erioboytrya japonica* leaf extracts, produced stable gold nanoparticles. This study showed green synthesis of AuNPs, as influential bioreduction of Au^{+3} utilizing *Erioboytrya japonica*, treating as reducing and stabilizing agents. Owing to the potential of E. *japonica* to be used as a reducing and stabilizing agents, it can be investigated using in the synthesis of other metal NPs. *Erioboytrya japonica* leaf extract exerted as medicinal values that may help to take adventage from the application in the future AuNPs in medicines.

Conflict of interest disclosure: The author declares no conflicts of interest.

References

Awwad AM, Salem, NM (2012) Green synthesis of silver nanoparticles by Mulberry leavesextrac. Nanosci Nanotechnol 2: 125–128.

Chen Y, Jingchun T, Xiaomei L, Xinwei R, Meinan Z, Lan W (2019) Green Biosynthesis of Silver Nanoparticles Using Eriobotrya japonica (Thunb.) Leaf Extract for Reductive Catalysis. Materials 12: 189.

Deljou A, Goudarzi S (2016) Green Extracellular Synthesis of the Silver Nanoparticles Using Thermophilic Bacillus Sp. AZ1 and its Antimicrobial Activity against Several Human Pathogenetic Bacteria. Iran J Biotechnol 14: 25–32.

Drummer S, Madzimbamuto T, Chowdhury M (2021) Green Synthesis of Transition-Metal Nanoparticles and Their Oxides: A Review. Mat 4:2700.

El-naggar ME, Shaheen TI, Fouda MMG, Hebeish AA (2016) Ecofriendly microwave-assisted green and rapid synthesis of well-stabilized gold and core–shell silver–gold nanoparticles. Carbohydr Polym 136:1128–36.

Hussain I, Singh NB, Singh A, Singh H, Singh SC (2016) Green synthesis of nanoparticles and its potential application. Biotechnol Lett 38: 545–560.

https://pfaf.org/user/plant.aspx?latinname=Eriobotrya+japonica

Kathiraven T, Sundaramanickam, A, Shanmugam, N, Balasubramanian T (2015) Green synthesis of silver nanoparticles using marine algae Caulerpa racemosa and their antibacterial activity against some human pathogens. Appl Nanosci 5:499–504.

Kharissova OV, Dias HR, Kharisov BI, Pérez BO, Pérez VMJ (2013) The greener synthesis of nanoparticles. Trends Biotechnol 31:240–248.

Madzimbamuto T, Chowdhury M, (2021) Green Synthesis of Transition-Metal Nanoparticles and Their Oxides: A Review. Materials 14: 2700.

Molnár Z, Bódai V, Szakacs G, Erdélyi B, Fogarassy Z, Sáfrán G, Varga, T, Kónya Z, Tóth-Szeles E, Sz″ ucs R.,et al (2018) Green synthesis of gold nanoparticles by thermophilic filamentous fungi. Sci Rep 8: 1–12.

Niknejad F, Nabili M, Ghazvini RD, Moazeni M (2015) Green synthesis of silver nanoparticles: Another honor for the yeast model Saccharomyces cerevisiae. Curr Med Mycol 1: 17–24.

Ovais M, Khalil AT, Islam NU, Ahmad I, Ayaz M, Saravanan M, Shinwari ZK, Mukherjee S (2018) Role of plant phytochemicals and microbial enzymes in biosynthesis of metallic nanoparticles. Appl Microbiol Biotechnol 102: 6799–6814.

Parveen M, Ahmad F, Malla AM, Azaz S (2016) Microwave-assisted green synthesis of silver nanoparticles from Fraxinus excelsior leaf extract and its antioxidant assay. Appl Nanosci 6:267–76.

Rastogi A, Singh P, Haraz FA, Barhoum A (2018) Biological synthesis of nanoparticles: An environmentally benign approach. Fundam Nanopart 571–604.

Ryaidh AH, Al-Qayim MAJ, (2017) Bio-Synthesis and Characterizations of Magnetic Iron Oxide Nanoparticles Mediated By Iraq Propolis Extract. IOSR J Pharm Biol Sci 12:65–73.

Sharma A, Dhiman N, Singh BP, Gathania, AK (2014) Green synthesis of gold nanoparticles using extracts of Artocarpus Lakoocha fruit and its leaves, and Eriobotrya Japonica leaves. Materials Research Express, 2053-1591.

Singh P, Kim, YJ, Zhang D, Yang DC (2016) Biological Synthesis of Nanoparticles from Plants and Microorganisms.Trends Biotechnol 34:588–599.

Singh V, Kumar P, Sanghi R (2012) Use of microwave irradiation in thegrafting modification of the polysaccharides–A review. Progress in Polymerscience 37(2): 340–360.

Sökmen, M., Alomar, S.Y., Albay, C., Serdar, G (2017) Microwave assisted production of silver nanoparticles using green tea extracts. Journal of Alloys and Compounds 725, 190-198.

Tanan W, Saengsuwan S (2014) Microwave assisted synthesis of poly(acrylamide-co-2-hydroxyethyl methacrylate)/poly(vinyl alcohol) semi-IPNhydrogel. Energy Procedia 56(0):386–393.

Torabfam M., Yüce M (2020) Microwave-assisted green synthesis of silver nanoparticles using dried extracts of Chlorella vulgaris and antibacterial activity studies. Green Processing and Synthesis 9: 283–293.

Zhao L, Chen J, Lv, H, Ao, XC, Ren, BR, Li WL (2015) A New Sesquiterpene Glycoside from the Leaves of Eriobotrya japonica. Chem Nat Compd 51:1103–1106.

RESEARCH ARTICLE
Bull Biotechnol (2021) 2(2):44-50
https://doi.org/10.51539/biotech.1032131 Jurnal homepage: www.dergipark.org.tr/biotech

Bulletin of Biotechnology

Biosynthesis of silver nanoparticles using extract of fig (*Ficus carica* L.) leaf by microwave extraction

Gönül Serdar

*Karadeniz Technical Universty, Central Research Laboratory,Trabzon,Türkiye

*Corresponding author : gonulserdar@ktu.edu.tr
Orcid No: : https://orcid.org/0000-0002-3589-2323

Received : 08/12/2021
Accepted : 27/12/2021

Abstract: Silver nanoparticles (AgNPs) were synthesized using extract of fig (*Ficus carica* L.) leaf and $AgNO_3$ solution by microwave method in this study. Freshly leaves of fig (*F. carica*.) were collected from the Eastern Black Sea region (Akçaabat-TRABZON) in Turkey and then dried. 25 g of dried sample was shaken in 500 mL of distilled water- citric acid (0.1 M) mixture (1:1) for 120 min at room temperature and extracted in a laboratoary microwave device at 5 minutes, 600 W and left cooling. Various volume of leaf extract (0.5,1,2,3 mL) was added $AgNO_3$ solution (1 mM-3 mM) and the mixture was exposed to a household microwave at 180W for 1–60 min for the biosynthesis of AgNPs. Silver nanoparticles were characterized using UV-visible absorption spectroscopy . The synthesis of AgNPs was observed by its colour changing from light yellow to dark brown and the characteristic plasmon resonance peak of silver nanoparticles was observed at around 400-500 nm.
Keywords: Silver nanoparticle, fig (*Ficus carica* L.) leaf, Green synthesis, MAE

1 Introduction

Nanotechnology is preferred technologies in recent years. Nanotechnology is interested of a size varying from 1 to 100 nm. Nanoparticles are significiant as they are common utilized in medical fields owing to their antibacterial activities nowadays. By means of their small size does it simple to permeate samples. Most researchers give importance to nanoparticles due to biomedical and environmental applications (Álvarez-Paino M et al. 2017;Muñoz-Bonilla et al.2019; Matar and Andac, 2020). Nanoparticles demonstrate broad utilize horizon in environmental preservation and other fields (Rónavári et al. 2017; Matar and Andac, 2020).The Nanostructures have various applications according as their distribution, size and morphology. It has implementations in different fields containg chemical industries, catalysis, biomedical, electronics, environment, cosmetics, health care, mechanics, photo-electrochemical and optics. There are two approaches, top-down and bottom-up for the synthesis of nanomaterials (Das et al. 2017). The use of toxic chemicals in the chemical and physical methods used ın order to biosynthesis of nanoparticles may pose potential hazards such as toxicity, carcinogenicity and environmental toxicity (Gupta and Xie 2018). Toxicity affairs are quite evident owing to the employ of danger substances such as organic solvents, stabilizers and reducing agents. The utilize of chemical contaminations and toxic solvents limits the use of nanoparticles in different biomedical and clinical applications (Hua et al. 2018). For this reason, It is necessary to use clean, reliable, biologically suitable and environmentally techniques, to biosynthesize nanoparticles. (Jain et al. 2010; Thakkar et al. 2010;Kulkarni and Muddapur 2014). There are two categories for "Natural" biogenic synthesis metallic nanoparticles; (a) Bioreduction, (b) Biosorption. The election of biological methods for synthesis of nanoparticles is releted to a few variables (Zhang et al. 2020).Fungi, bacteria and plant leaves are utilized so as to the biosynthesis of gold and silver nanoparticles (Ulug et al. 2015). Nowadays, Biological methods using plants and microorganisms are preferred than Physical and chemical methods which were expensive and toxic (Horsfall, 2014; Matar and Andac, 2020). Plant leaves has important advantages such as, simplicity, ease of preparation, health, environmental care and nanoparticle formation rate. Plant leaves used for the formation of silver nanoparticles (AgNPs) display fast growth and diversity. These extracts comprise the necessary agents for capping the reduced NPs and the reduction of silver ions (Ulug et al. 2015). Silver nanoparticles (AgNPs) which were different sizes, charges and properties can be used in different applications toxic (Matar and Andac, 2020).Silver nanoparticles (AgNPs) have obtained important interest owing to their application towards biomolecular, therapeutics, waste management, catalysis

(Joseph and Mathew 2015), drug delivery, (Jagtap and Bapat 2013; Mashwani et al. 2015) and cost effective synthesis. these properties usually subjected to the surface area, morphology, capping sheet, and particle size of nanoparticles (Zheng et al.; Oh et al. 2009; Courty, 2010). Hence, it is essential to improve environmental friendly ,a cost effective and synthetic route to prepare AgNPs. Nowadays, the silver nanoparticles (AgNPs) have point out attention owing to their active sensor and optical properties (Ghosh and Pal 2007; Han and Li 2010). Furthermore, AgNPs display well antimicrobial potential activity and biocompatibility than other nanoparticles (Jagtap and Bapat 2013; Mashwani et al. 2015). The fig is the fruit of fig (*Ficus carica*) leaf, a species of family Moraceae. It is now widely grown throughout the world and ıts native to the Mediterranean and western Asia. Figs include various phytochemicals containing polyphenols, such as chlorogenic acid, gallic acid, (+)-catechin, (−)-epicatechin, syringic acid and rutin (Vinson, 1999; Veberic et al. 2018). The microwave-assisted synthesis method produces NPs with lower dispersion, which is arranged in a more regular pattern. It is noteworthy that the shape and morphology of the formed nanostructures can be controlled in this procedure (Parveen et al. 2020;Torabfam and Yüce,2020). I used this plant in this study because it acts as a bioreductant and it is also that readily available from anywhere in the world. The aim of this work was to synthese the AuNPs by using Fig (*Ficus carica*) leaves extract as a reducing agent which were processed in MAE method.

2 Materials and Method

2.1 Materials

Fig (*F. carica*) Leaves were collected from Trabzon city, Turkey. Respectivelly the leaves were washed with deionized water, air-dried for 3-5 days, and then the dried leaves were pulverized in a grinder and stored for use. Silver nitrate was provided from Sigma Aldrich. Before the experiments, glasswares were cleaned with deionized water.

2.2 Preparation of extract

Fig (*F. carica*) leaves were wash using deionized water and cut into small pieces. The Fig leaves pieces were dried and ground to powder later. Then, 25 gram of dried Fig (*F. carica*) leaves powder was shaken in 500 mL of distilled water- citric acid (0.1 M) mixture (1:1) for 120 minutes at 25 ºC and then extracted in a laboratoary microwave device at 5 minutes, 600 W. The mixture was filtered Whatmann No. 1 filter paper, then the filtrate was kept at 4 °C so as to be utilized for the synthesis of AgNPs experiments.

2.3 Synthesis of silver nanoparticles

To obtain AgNPs, various volume of leaf extract (0.5,1,2,3 mL) was added $AgNO_3$ solution (1 mM, 2 mM, 3 mM). The mixture was subjected to a household microwave at 180W for 1–60 minutes for the biosynthesis of AgNPs to find the optimum reaction parameters. The prepared nanoparticles solution was stored at room temperature for the further experiment. The color variation from colorless to light yellow/brown following application of the microwave is an indication of colloidal AgNP in solution. The volumes of extract and concentrations of silver nitrate solutions were optimized for synthesis of silver nanoparticles (AgNPs). Each procedure was attempted three times. The concentrations and volumes of the substances used in the synthesis of silver nanoparticles are given in Table 1.

Table 1: Composition of AgNPs

Fig leaf Extract(mL)	$AgNO_3$(mM)
0.5	1
1	1
2	1
3	1
0.5	2
1	2
2	2
3	2
0.5	3
1	3
2	3
3	3

2.4 Characterization

The reduction of Ag^+ to Ag^0 was carried out by taking a certain amount of each reaction mixture in the range of 300 to 800 nm at 1 nm resolution via the spectral data of the UV-vis spectrophotometer (Shimadzu UVP-1240). The spectra of Fig (*F. carica*) leaves extracts and $AgNO_3$ solution were taken. Deionised water was used to adjust the baseline as a blank. A characteristic surface plasmon resonance (SPR) band absorption peak of silver nanoparticles came out between 410 and 480 nm (Mulvaney 1996; Das et al. 2010). The intensity and width of the peak are related to the particle size distribution. So far as the theory, merely a single SPR band peak is expected for the absorption spectra of spherical nanoparticles, however anisotropic nanostructures of spherical nanoparticlesmay result to two or more SPR bands according as the shape of the particles (Sökmen et al. 2017).

2.5 Statistical analysis

The values which were derived from experiments are exhibited in the study as means ± standard deviation (SD)

3 Results and Discussion

The color change of the solutions from pale yellow to yellowish brown is a powerful sign of nanoparticle (Fig 1.) Spectrophotometric screening of fig *(F. carica)* leaf extract (0.5,1,2,3 mL) and $AgNO_3$ solution (1 mM, 2 mM, 3 mM) mixture) after a household microwave treatment were realized for several periods. The UV-visible spectrum of AgNPs is exhibited in figure 2,3,4 between 300–800 nm. SPR absorption spectra of silver nanoparticles generated from 1 mM (Fig.2), 2 mM (Fig.3) and 3 mM (Fig.4) $AgNO_3$ concentration.

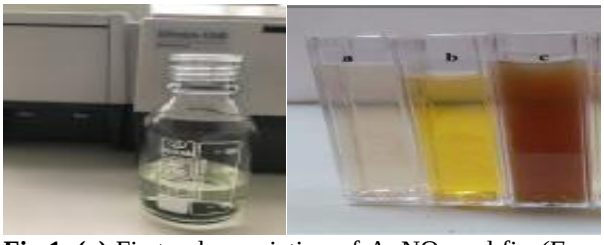

Fig 1. (a) First **c**olor variation of $AgNO_3$ and fig *(F. carica)* leaves extract mixture, **(b and c)** color change after microwave treatment.

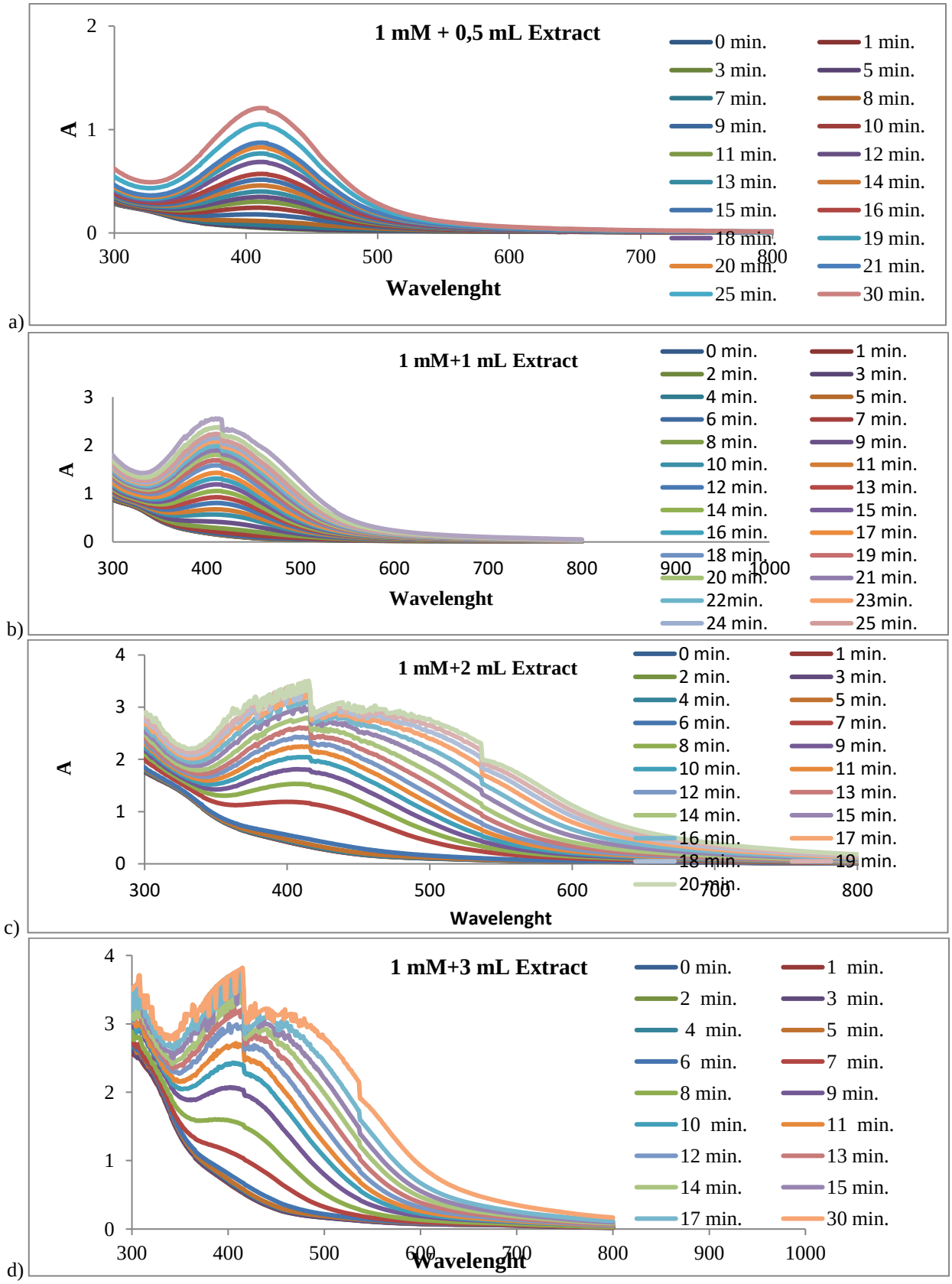

Fig 2 (a),(b),(c),(d). SPR absorption spectra of silver nanoparticles produced from different volume of 1 mM $AgNO_3$

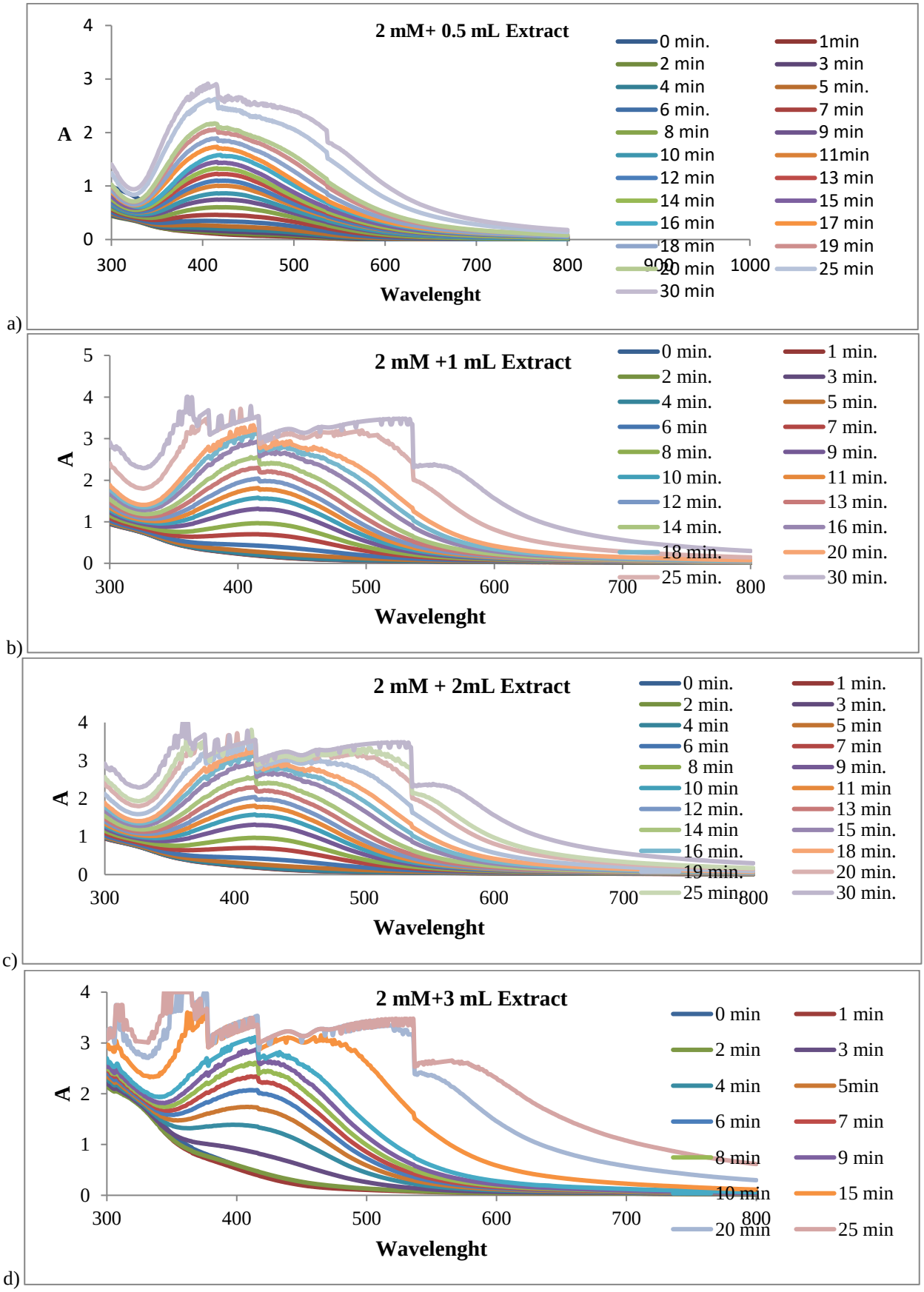

Fig 3 (a),(b),(c),(d). SPR absorption spectra of silver nanoparticles produced from different volume of 2 mM $AgNO_3$.

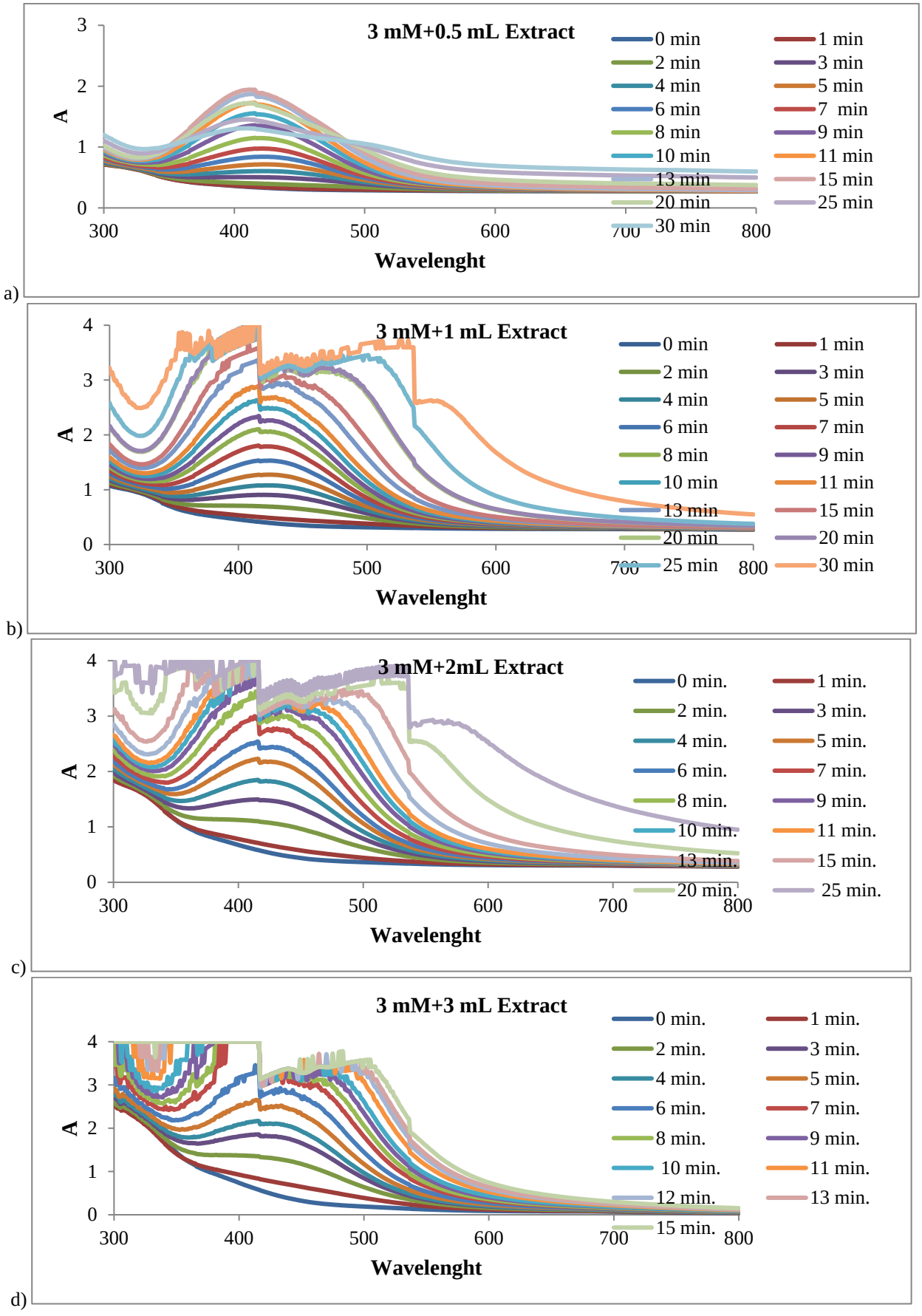

Fig 4 (a),(b),(c),(d). SPR absorption spectra of silver nanoparticles produced from different volume of 3 mM $AgNO_3$.

The formation of silver nanoparticles as color change is owing to the excitation of surface plasmon vibration of silver nanoparticles (Sökmen et al. 2017). According to Fig. 2., AgNPs were produced with 0.5 and 1 mL of fig leaf extract (Fig. 2a and b) as specific resonance band observed between 400-500 nm after 18 and 15 minutes of microwave, respectively. The band attained maximum height after 30 minutes of microwave processing at 180 W (Fig. 2a). High extract volume (2 mL and 3 mL) increased the number of nanoparticles. Particle size as a consequence of agglomeration is seen from the brownish, cloudy color of the reaction mixture and from the spectra given in Fig. 2c and d. The same production procedure was repeated for 2 mM and 3 mM $AgNO_3$ concentrations. Findings are given in Figure 3 (2 mM) and Figure 4 (3 mM).

AgNPs were successfully produced as seen in Fig. 3 and Fig. 4. The wider resonance band showed the formation of larger nanoparticles. AgNO3 concentration was increased and other parameters were kept the same. Furthermore, 3 mL of fig *(F. carica)* extract appears to produce AgNPs even after 4 min of microwave treatment (Fig. 3d and 4d) and a band peak shift was observed in the 500 nm region. The peak intensity and full width at half maximum subjects to extent and size of aggregation of particles. Thus, the broadness of the peak in all cases may be predicated to the broad particle size distribution

4 Conclusions

An economical, simple and fast production of AgNP was descriped in our work. Utilizing fig *(F. carica)* leaf extracts, fabricated stable silver nanoparticles. No capping agent was needed as aggregation was prevented by the extract. Using the microwave process makes nanoparticle production easier. biomolecules present in fig *(F. carica)* extract are able to reduce silver ions to silver nanoparticles. Fig *(F. carica)* extract contains biomolecules and thus can reduce silver ions to silver nanoparticles. This study showed a simple green synthesis of AgNPs by effective biological reduction of Ag+ using *F. carica*, reducing agents. Microwave irradiation was utilized as a good energy source by place of other time-consuming energy supplies. Alongside the significant progress in nanobiotechnology, more futuristic opinions in nanoscience inclueds of the broad utilize of NPs in biomedical and pharmaceutical applications.

References

Álvarez-Paino M, Muñoz-Bonilla A, Fernández-García M (2017) Antimicrobial polymers in the nano-world. Nanomaterials 7(2):48

Courty A (2010) Silver nanocrystals: self-organization and collective properties. J Phys Chem C 114:3719–3731.

Das RK, Pachapur VL, Lonappan L, Naghdi M, Pulicharla R, Maiti S (2017) Biological synthesis of metallic nanoparticles:plants, animals and microbial aspects. Nanotechnol Environ Eng 2:18.

Dwivedi P, Narvi SS, Tewari RP (2014) Phytofabrication characterization and comparative analysis of Agnanoparticles by diverse biochemicals from Elaeocarpus ganitrus Roxb., Terminalia arjuna Roxb., Pseudotsuga menzietii, Prosopisspicigera, Ficus religiosa, Ocimum sanctum, Curcuma longa. Ind Crops Prod 54: 22–31.

Gupta R, Xie H (2018) Nanoparticles in daily life: applications,toxicity and regulations. J. Environ. Pathol Toxicol Oncol 37: 209–230.

Ghosh SK, Pal T (2007) Interparticle coupling effect on the surface plasmon resonance of gold nanoparticles: from theory to applications. Chem Rev 107:4797–4862.

Han CP, Li HB (2010) Host-molecule-coated quantum dots as flurescent sensor. Anal Bioanal Chem 397:1437–1444.

Horsfall L (2014) Biological synthesis of metallic nanoparticles by bacteria, fungi and plants. J

Nanomed Nanotechnol 5(5):1

Hua S, de Matos, MBC, Metselaar, J M, Storm G (2018) Current trends and challenges in the clinical translation of nanoparticulate nanomedicines:pathways for translational development and commercialization. Front Pharmacol 9:790.

Jagtap UB, Bapat VA (2013) Green synthesis of silver nanoparticles using Artocarpus heterophyllus Lam. seed extract and its antibacterial activity. Ind Crop Prod 46:132–137.

Jain, N., Bhargava, A., Majumdar, S., Tarafdar, J., and Panwar J (2010) Extracellular biosynthesis and characterization of silver nanoparticles using aspergillus flavusNJP08: a mechanism perspective. Nanoscale 3:635–641.

Joseph S, Mathew B (2015) Microwave-assisted green synthesis of silver nanoparticles and the study on catalytic activity in the degradation of dyes. J Mol Liquids, 204:184–191

Kalam A, Al Sehemi AG, Alrumman S, Du G, Pannipara M, Assiri M, Almalki H, Mahmoud F, Moustafa (2017) Colorimetric Sensing of Toxic Metal and Antibacterial Studies by Using Bioextract Synthesized Silver Nanoparticles. J Fluoresc 27:2045–2050.

Kulkarni N, Muddapur U (2014) Biosynthesis of metal nanoparticles: a review. J Nanotechnol 2014:510246.

Mashwani ZU, Khan T, KhanMA, Nadhman A (2015) Synthesis in plants and plant extracts of silver nanoparticles with potent antimicrobial properties: current status and future prospects. Appl Microbiol Biotechnol 99:9923–9934.

Matar GH, Andac, M (2020) Antibacterial efficiency of silver nanoparticles-loaded locust bean gum/polyvinyl alcohol hydrogels. Polymer Bulletin,2020, 78, 6095–6113.

Muñoz-Bonilla A, Echeverria C, Sonseca Á, Arrieta MP, Fernández-García M (2019) Bio-based polymers with antimicrobial properties towards sustainable development. Materials 12(4):641

Oh N, Kim JH, Jin S, Yoon CS (2009) Reversible size-tuning of self-assembled silver nanoparticles in phospholipid membranes via humidity control. Small 5:1311–1317.

Parveen M, Ahmad F, Malla AM, Azaz S (2016) Microwave-assisted green synthesis of silver nanoparticles from Fraxinus excelsior leaf extract and its antioxidant assay. Appl Nanosci 6:267–76.

Rónavári A, Kovács D, Igaz N, Vágvölgyi C, Boros IM, Kónya Z, Pfeiffer I, Kiricsi M (2017) Biological activity of green-synthesized silver nanoparticles depends on the applied natural extracts: a comprehensive study. Int J Nanomed 12, 871–883.

Sökmen, M., Alomar, S.Y., Albay, C., Serdar, G (2017) Microwave assisted production of silver nanoparticles using green tea extracts. J Alloys Compd 725: 190-198.

Thakkar KN, Mhatre SS, Parikh RY (2010) Biologicalsynthesis of metallic nanoparticles. Nanomedicine 6: 257–262.

Torabfam M and Yüce M, 2020.Microwave-assisted green synthesis of silver nanoparticles using dried extracts of Chlorella vulgaris and antibacterial activity studies. Green Processing and Synthesis, 9: 283–293.

Ulug B, Turkdemir MH, Cicek A, Mete A (2015) Role of irradiation in the green synthesis of silver nanoparticles mediated by fig

(Ficus carica) leaf extract Spectrochimica Acta Part A: Molecular and Biomolecular Spectroscopy 135:153–161.
Veberic R, Colaric M, Stampar F (2008) Phenolic acids and flavonoids of fig fruit (Ficus carica L.) in the northern Mediterranean region. Food CheM 106 (1): 153–157.
Vinson JA (1999) The functional food properties of figs. Cereal Food World 4: 82-87.
Zhang D, Ma X-l, Gu Y, Huang H and Zhang G-W (2020) Green Synthesis of Metallic Nanoparticles and Their Potential Applications to Treat Cancer. Front Chem 8:799.
Zheng J, Nicovich PR, Dickson RM (2007) Highly fluorescent noble-metal quantum dots. Annu Rev Phys Chem 58:409-431.

RESEARCH ARTICLE
Bull Biotechnol (2021) 2(2):51-55
https://doi.org/10.51539/biotech.1032945 Jurnal homepage: www.dergipark.org.tr/biotech

Bulletin of Biotechnology

Evaluation of the bioaccessibility of peanut skin polyphenols and their potential use for food enrichment

Bige Incedayi*, Nihal Türkmen Erol

* *Bursa Uludag University, Faculty of Agriculture, Department of Food Engineering, 16059, Bursa, Turkey*

*Corresponding author *:* bige@uludag.edu.tr
Orcid No: https://orcid.org/0000-0001-6128-7453

Received : 06/12/2021
Accepted : 29/12/2021

Abstract: Polyphenols obtained from agricultural and industrial residues are also considered as remarkable sources of natural antioxidants to replace synthetic ingredients. In this study, the contents of total polyphenols (TP) and total flavonoids (TF), antioxidant capacity (AC) and *in-vitro* bioaccessibility of polyphenols (as gastric and intestinal stages) of the extract from peanut skin using water were investigated. Additionally, the potential use of peanut skin extract in noodle production was researched in order to add functionality to noodle, which is a widely consumed product. The results showed that 71.67 mg gallic acid equivalent (GAE)/g dry matter (DM) of TP, 123.11 mg rutin equivalent (RE)/g DM of TF and 66267.46 mmol ascorbic acid equivalent (AAE)/100g DM of AC were found in peanut skin. After the gastric and intestinal stages, the TP content and AC of the skin extract were found to be lower than the initial (before digestion) value. It was determined that polyphenols were more stable in gastric conditions than in the small intestine. The addition of the skin extract (0.4%) to the noodle dough increased the TP and AC of the final product compared to the noodle without the skin extract (control). It was observed that the stability of the polyphenols from the noodle sample was higher in gastric stage than intestinal one. The addition of peanut skin extract to the noodle dough increased the bioaccessibility of the polyphenols. Therefore, this study showed that peanut skin, as an important source of polyphenols, may be useful for food enrichment.

Keywords: peanut skin; polyphenol; *in-vitro* digestion; noodle

1 Introduction

During vegetative processing, a significant amount of wastes rich in polyphenols with antioxidant activity is generated. In recent years, due to environmental factors and economic reasons, studies about valorization of these wastes have increased gradually. As a result of the processing of peanut fruit (*Arachis hypogaea* L.), a large amount of red-pink colored skin is produced as waste, and they are generally used as animal feed, fertilizer and fuel (Yu et al. 2005; Win et al. 2011). Previous studies have shown that peanut skin is a rich source of bioactive polyphenols (Larrauri et al. 2016). The use of extracts from plants or their by-products containing bioactive substances such as phenolic compounds in various foods as an alternative to artificial additives or for food enrichment is increasing gradually. According to Amado et al. (2014) found that the extract from potato peel waste prevented oxidation in soybean oil due to its antioxidant activity. Rashidinejad et al. (2016) reported that both the total polyphenols and the total antioxidant capacity of cheeses obtained by adding green tea catechins to whole milk increased. While an increase in phenolic content and antioxidant activity of fresh pasta enriched with extract from artichoke waste was observed, the extract decreased yellowness and increased brownness but did not change the textural and cooking parameters (Pasqualone et al. 2017). On the other hand, there is no study on the use of peanut skin extract in foods; but only, in the study conducted by Ma et al. (2014), ground peanut skin was added to peanut butter.

Although phenolic compounds have strong antioxidant activity, their bioactivity depends on their degree of bioaccessibility (Wang et al. 2017). The release of compounds from food and their solubility during digestion are called bioaccessibility, and a high rate of bioaccessibility is required for intestinal absorption of these compounds. Assessing the actual bioavailability of a phenolic compound in the human or animal body is difficult and costly. Instead, the *in-vitro* gastrointestinal digestion method is a simpler and faster method used to obtain information about the release of a phenolic compound from the foodstuff and its stability in gastrointestinal conditions. In some previous studies conducted on different materials such as pomegranate peel flour (Gullon et al. 2015), cocoa powder (Gìltekin-Özgìven et

al. 2016), apple (Bouayed et al. 2012) and elderberry fruit (Pinto et al. 2017), the bioaccessibility of phenolic compounds was determined according to the *in-vitro* gastrointestinal digestion method, but in the literature, there has been no study on the bioaccessibility of peanut skin polyphenols.

In this study, it was aimed to (1) determine the total polyphenols (TP), total flavonoids (TF) and antioxidant capacity (AC) of the extract from peanut skin, and the bioaccessibility of polyphenols (2) use peanut skin extract for enrichment in noodle production and thus to evaluate peanut skin, which is an important waste.

2 Materials and Method

2.1 Materials

The skins of peanut (*Arachis hypogaea* L.) used in the study were supplied from a peanut processing plant (Ece Tarım, Aydın, Turkey). They were stored in polyethylene bags at 4±2ºC until used. Flour and eggs were obtained from the local market.

2.2 Polyphenol extraction

Polyphenols were extracted from ground powder skin and noodles (both with and without the skin extract) with a certain particle size (150-300 µm) using distilled water at solid to solvent ratio of 1/39.70 (w/v) and temperature of 60°C for 22 min. The use of water has several advantages over commonly used organic solvents since it is an environmentally-friendly solvent with remarkable extraction capacity and no toxicity for human health (Chen et al. 2013). After extraction, the mixture was rapidly cooled under tap water, centrifuged at 10 000 rpm for 15 min and filtered through Whatman No.1 filter paper. The clear extract was stored at –20°C until used for analyses of TP, TF, AC and bioaccessibility. Some part of the extract was also stored at –80°C for freeze-drying (at –50ºC and under 0.1 mbar/0.75 mmHg vacuum) to use in noodle production. Each extraction was carried out in triplicate.

2.3 Determination of total polyphenol (TP)

TP of the extract or pure water (as a blank) was determined using the Folin-Ciocalteu method (ISO 14502-1:2005). The blue color of the reaction mixture was measured at 765 nm against blank using a spectrophotometer (Shimadzu UV-VIS 1208). A calibration curve of gallic acid (5-50 µg/mL) was prepared and the results determined from regression equation of the calibration curve (R^2=0.99) were expressed as mg gallic acid equivalents (GAE) per gram of dry matter (DM).

2.4 Determination of total flavonoid (TF)

The amount of TF was determined by spectrophotometric method (Rodrigues et al. 2016). Rutin (0-1500 ppm; R^2= 0.99) was used as a standard and a standard curve was obtained with its different concentrations at 510 nm. Results were calculated based on this curve and expressed as mg rutin equivalents per gram of dry matter (mg RE/g DM).

2.5 Antioxidant capacity (AC)

AC was determined by the 2,2,diphenyl-2-picryl-hydrazyl (DPPH) method of Türkmen Erol et al. (2009) at 517 nm. AC was calculated as percentage inhibition (AC, %) of the DPPH radical by the following equation:

$$AC(\%) = \frac{Abs_{control} - Abs_{sample}}{Abs_{control}} x100$$

Abscontrol: Absorbance of the solution of DPPH without sample,

Abssample: Absorbance of the solution of DPPH with sample

AC (%) of samples was converted to ascorbic acid equivalent (AAE) defined as mmol of ascorbic acid equivalents per 100 g of DM.

2.6 *In-vitro* digestion (Bioaccessibility)

In-vitro digestion method was applied according to Minekus et al. (2014) to evaluate the bioaccessibility of phenolic compounds of the sample extracts. It was carried out in two stages as gastric and intestinal. After each stage, the amount of TP was determined by spectrophotometer and the bioaccessibility (%) of TP was calculated as follows.

Bioaccessibility (%) = ($C_{digested}$ / $C_{undigested}$) x 100

C digested: Concentration in digested sample after gastric/intestinal stage (mg)

C undigested: Concentration in undigested sample (mg)

2.7 Noodle production

Noodle production was carried out according to Collins and Pangloli (1997) with some modification. The freeze-dried extract was used at a rate of 0.4% in noodle production. The ratios of other ingredients were 65%, 21.6% and 13% for flour, water and egg, respectively. Noodle without skin extract formed the control group. Dry ingredients (wheat flour and dry extract) were combined and mixed in a bowl. Then, water and egg were added and the mixture was kneaded for 5 min using a dough mixer (Siemens FQ.1) until the dough stiffened. After that, the dough was hand-kneaded for 5 more min, divided into equal portions (shaped into a ball), wrapped with cling film and allowed to rest for 20 min at room temperature. At the end of the period, the dough was thinned first with a roller and then with a dough thinning machine (Titania, Italy). Dough was rested for 20 min at room temperature in order to remove excess moisture and thus prevent sticking that may occur during cutting. Then, the dough was cut into strips of 0.4 x 3 cm in two stages with a noodle cutting machine. Fresh noodles were spread on trays and dried at room temperature until the moisture content of noodle decreased to 8-9%. Dry noodles were stored at the same temperature in polyethylene bags until analysis.

Fig. 1 Dough mixer and thinning machine

2.8 Statistical analysis

Experimental results were expressed as means ± standard deviation of triplicate measurements and analyzed by SPSS software (SPSS statistics 23, IBM.2015). Analysis of variance was performed by one-way ANOVA procedure. Means were compared by using Duncan multiple comparison test. Values of $p < 0.05$ were considered as significantly different.

3 Results and discussion

3.1 The effect of *in-vitro* digestion on TP and AC of peanut skin extract

TP and AC values of peanut skin extract at initial and after digestion are given in Table 1. TP value (71.67 mg GAE/g DM) found in this study was less than that reported by Win et al. (2011) (91.74 mg GAE/g) for peanut skin. This dissimilarity can be due to the differences in the extraction solvent, the analysis method and the standard used. When the TP value from this study was compared with the values of other plant by-products; 9.18 mg GAE/g hazelnut skin (Stevigny et al. 2007), 7.51-18.51 mg GAE/g dw (Zardo et al. 2019) for sunflower seed meal and a maximum of 1.13 mg GAE/g dw (Amado et al. 2014) for potato peel waste were reported. These results showed that the peanut skin is an important source of polyphenols. On the other hand, the result of AC (66267.46 mmol AAE/100g DM) from this study was not possible to compare to the literature values because of the fact that the same antioxidant method used in the studies was applied with different modifications and the results were expressed in different units. For example; 309 - 1375 µmol Trolox equivalent-TE/g skin (Taş and Gökmen 2015) and 854.47- 1004.98 µM TE/g dw (Bertolino et al. 2015) in hazelnut skin and 2077- 5214 µmol TE/kg fresh weight (Punzi et al. 2014) in artichoke waste and 3.24 mmol TE/g extract (Vázquez et al. 2012) in chestnut bark were detected.

The TP and AC of the skin extract showed a similar trend after digestion. They both significantly decreased compared to their initial values ($p < 0.05$) (Table 1). The highest decrease was observed in the intestinal phase. This is associated with lower stability of polyphenols due to the alkaline environment during intestinal digestion (Fawole and Opara 2016). The reduction of TP and thus AC after gastrointestinal digestion has also been demonstrated in the previous studies with different foods. Bouayed et al. (2012) stated that the TP content of four different apple cultivars (with an average initial TP level of 44.42 mg/100 g fresh weight) decreased to 35.95 mg/100 g fresh weight after the gastric stage and to 21.84 mg/100 g fresh weight after the pancreatic stage. Similarly, TP and AC values of ten different walnut varieties decreased by an average of 74.1% and 77%, respectively, after *in-vitro* digestion compared to their initial values (Figueroa et al. 2016).

However, unlike these results, Wang et al. (2017) reported that TP and AC of grape pomace did not change after the gastric digestion, but decreased after the intestinal digestion compared to their initial values. According to the results of a study conducted with pomegranate products and wastes, the initial TP and AC values showed different trends after *in-vitro* digestion, depending on the material and the extraction solvent used. With respect to TP, both a decrease and an increase were observed at the end of both stages, while a decrease at the end of the gastric stage and an increase at the end of the intestinal stage were observed regarding AC (Fawole and Opara 2016). The differences in the results might be due to the differences in stability of the polyphenols of the materials used and *in-vitro* digestion conditions applied.

Table 1 TP, bioaccessibility of TP and AC values of peanut skin

	Initial	Gastric	Intestinal
TP (mg GAE/g DM)	$71.67 \pm 1.32^{c*}$	50.00 ± 0.59^{b}	33.41 ± 0.73^{a}
AC (mmol AAE/100g DM)	66267.46 ± 404.69^{c}	36276.52 ± 463.26^{b}	25940.40 ± 1453.22^{a}
Bioaccessibility of TP (%)	100.00 ± 0.00^{c}	69.82 ± 1.62^{b}	46.62 ± 0.85^{a}

*The differences between means in lower case letters in the same row are significant ($p < 0.05$).

3.2 The effect of *in-vitro* digestion on TP and AC of noodle

In order to obtain enriched noodle, peanut skin extract was freeze-dried and added to the noodle dough. According to the results of the analysis, the addition of the extract significantly increased (50.94%) the TP content of the enriched noodle compared to the control one, as expected (Table 2). While AC was not detected in the control noodle, it was determined at the level of 221.45 mmol AAE/100g DM in the enriched noodle. The results obtained from the previous studies in which noodle (Kazemi et al. 2017) and fresh noodle (Pasqualone et al. 2017) were enriched with pomegranate peel and artichoke waste extracts, respectively, were in agreement with the results of this study. However, the researchers found a lesser increase compared to this study. This could be due to the differences in the stability of the polyphenols of pomegranate peel (72.21 mg GAE/g; Ranjha et al. 2020) and artichoke waste (0.77-1.45 mg GAE/g fresh weight; Punzi et al. 2014) and noodle processing conditions (kneading, thinning and drying, etc.).

In-vitro digestion significantly affected the TP content and AC of the noodle samples ($p < 0.05$) (Table 2). The TP content of the control and enriched noodle samples showed a significant decrease ($p < 0.05$) after digestion, but more at the intestinal stage, as in the TP of the skin extract. Already, it is stated that polyphenols are sensitive to environmental factors such as pH change, light and heat, and are easily degraded by digestive enzymes (Pinto et al. 2017). On the other hand, it was observed that the bioaccessibility of noodle polyphenols was higher than the peanut skin polyphenols. This could be due to binding of polyphenols to the proteins in the composition of the noodle, increasing their stability during digestion (Xiong et al. 2020). In addition, the bioaccessibility of the polyphenols of the enriched noodle was higher than that of the control one (Table 2). After *in-vitro* digestion, the AC of the enriched noodle was also significantly decreased due to the decrease in its TP content ($p < 0.05$). So, it had no AC after the intestinal stage.

Table 2 TP, bioaccessibility of TP and AC values of noodle

	Noodle	Digestion Stage		
		Initial	Gastric	Intestinal
TP (mg GAE/g DM)	Control	0.53±0.03^{c*}	0.29±0.01^{b}	0.12±0.01^{a}
	Enriched	0.80±0.01^{b}	0.60±0.03^{a}	0.56±0.04^{a}
Bioaccessibility of TP (%)	Control	100.00±0.00^{c}	53.75±1.81^{b}	22.27±2.64^{a}
	Enriched	100.00±0.00^{b}	74.08±3.06^{a}	69.88±5.09^{a}
AC (mmol AAE/100g DM)	Control	0	0	0
	Enriched	221.45±11.25^{b}	19.53±0.35^{a}	0

*The differences between means in lower case letters in the same row are significant ($p < 0.05$).

3.3 TF content of skin and noodles

The TF content of the peanut skin and noodle samples is shown in Table 3. More TF (123.11 mg RE/g DM) than TP was found in the peanut skin. In some previous studies, TF content was found to be 12.4-36.22 mg quercetin equivalent (QE)/g extract (Larrauri et al. 2016) in peanut shell, 47.41-166.28 mg catechin equivalent (CE)/g skin extract (Ham et al. 2015) and 12.28 mg/100 g skin extract (Lee et al. 2016) in chestnut shell. However, since the results of the researchers were expressed using different standard phenolics and in different units, a comparison could not be made with the result of this study. According to the Table 3, the addition of peanut skin extract to the noodle dough increased the TF content of the enriched noodle (328.57%) compared to the control one as in the TP content. Consistent with this result, Mir et al. (2017) observed an increase in its TF content by adding apple pulp to the composition of crackers made from rice flour.

Table 3 TF content (mg RE/g DM) of the peanut skin and noodles

Skin extract	123.11 ± 0.32^{c*}
Control noodle	0.35 ± 0.02^{a}
Enriched noodle	1.50 ±0.03^{b}

* : The differences between means in lower case letters in the same column are significant ($p < 0.05$).

4 Conclusions

Peanut skin was evaluated in terms of TP, bioaccessibility of polyphenols, TF and AC. Due to the high TP content of the peanut skin, the extract from the skin was freeze-dried for use in the noodle formulation. It was determined that the noodle enriched with the peanut skin extract contained higher amount of TP and TF compared to the control noodle, and therefore, the enriched noodle showed AC although it could not be detected in the control one. On the other hand, the amount of TP and AC of the skin and noodles decreased significantly during *in-vitro* digestion, but more at the intestinal stage ($p < 0.05$). However, this decrease was less in noodles due to their protein content. The results obtained from this study showed that peanut skin can be used as a rich source of polyphenols for food enrichment.

Authors' contributions: Both authors contributed equally.

Conflict of interest disclosure:

There is no conflict of interest.

References

Amado IR, Franco D, Sánchez M, Zapata C, Vázquez JA (2014) Optimisation of antioxidant extraction from *Solanum tuberosum* potato peel waste by surface response methodology. Food Chem 165:290–299. https://doi.org/10.1016/j.foodchem.2014.05.103

Bertolino M, Belviso S, Dal Bello B, Ghirardello D, Giordano M, Rolle L, Gerbi V, Zeppa G (2015) Influence of the addition of different hazelnut skins on the physicochemical, antioxidant, polyphenol and sensory properties ofyogurt. LWT - Food Sci Technol 63:1145–1154. https://doi.org/10.1016/j.lwt.2015.03.113

Bouayed J, Deußer H, Hoffmann L, Bohn T (2012) Bioaccessible and dialysable polyphenols in selected apple varieties following in vitro digestion vs. their native patterns. Food Chem 131:1466–1472. https://doi.org/10.1016/j.foodchem.2011.10.030

Chen XX, Wu XB, Chai WM, Feng HL, Shi Y, Zhou HT, Chen QX (2013) Optimization of extraction of phenolics from leaves of Ficus virens. J. Zhejiang Univ. Sci. B (Biomedicine Biotechnol. 14: 903–915. https://doi.org/10.1631/jzus.B1200365

Collins JL, Pangloli P (1997) Chemical, physical and sensory attributes of noodles with added sweet potato and soy flour. J Food Sci 62:622–625. https://doi.org/10.1111/j.1365-2621.1997.tb04446.x

Fawole OA, Opara UL (2016) Stability of total phenolic concentration and antioxidant capacity of extracts from pomegranate co-products subjected to in vitro digestion. BMC Complement Altern Med 16:1–10. https://doi.org/10.1186/s12906-016-1343-2

Figueroa F, Marhuenda J, Zafrilla P, Martínez-Cachá A, Mulero J, Cerdá B (2016) Total phenolics content, bioavailability and antioxidant capacity of 10 different genotypes of walnut (*Juglans regia* L.). J Food Nutr Res 55:229–236

Gìltekin-Özgìven M, Berktaş I, Özçelik B (2016) Change in stability of procyanidins, antioxidant capacity and in-vitro bioaccessibility during processing of cocoa powder from cocoa beans. LWT - Food Sci Technol 72:559–565. https://doi.org/10.1016/j.lwt.2016.04.065

Gullon B, Pintado ME, Fernández-López J, Pérez-Álvarez JA, Viuda-Martos M (2015) In vitro gastrointestinal digestion of pomegranate peel (*Punica granatum*) flour obtained from co-products: Changes in the antioxidant potential and bioactive compounds stability. J Funct Foods 19:617–628. https://doi.org/10.1016/j.jff.2015.09.056

Ham JS, Kim HY, Lim ST (2015) Antioxidant and deodorizing activities of phenolic components in chestnut inner shell extracts. Ind Crops Prod 73:99–105. https://doi.org/10.1016/j.indcrop.2015.04.017

ISO 14502-1:2005 Determination of substances characteristic of green and black tea. Part 1: Content of total polyphenols in tea. Colorimetric method using Folin-Ciocalteu reagent. 8p.

Kazemi M, Karim R, Mirhosseini H, Hamid AA, Tamnak S (2017) Processing of Parboiled Wheat Noodles Fortified with Pulsed

Ultrasound Pomegranate (*Punica granatum* L. var. Malas) Peel Extract. Food Bioprocess Technol 10:379–393. https://doi.org/10.1007/s11947-016-1825-8

Larrauri M, Zunino MP, Zygadlo JA, Grosso NR, Nepote V (2016) Chemical characterization and antioxidant properties of fractions separated from extract of peanut skin derived from different industrial processes. Ind Crops Prod 94:964–971. https://doi.org/10.1016/j.indcrop.2016.09.066

Lee NK, Jung BS, Na DS, Yu HH, Kim JS, Paik HD (2016) The impact of antimicrobial effect of chestnut inner shell extracts against *Campylobacter jejuni* in chicken meat. LWT - Food Sci Technol 65:746–750. https://doi.org/10.1016/j.lwt.2015.09.004

Ma Y, Kerr WL, Swanson RB, Hargrove JL, Pegg RB (2014) Peanut skins-fortified peanut butters: Effect of processing on the phenolics content, fibre content and antioxidant activity. Food Chem 145:883–891. https://doi.org/10.1016/j.foodchem.2013.08.125

Minekus M, Alminger M, Alvito P, Ballance S, Bohn T, Bourlieu C, Carrière F, Boutrou R, Corredig M, Dupont D, Dufour C, Egger L, Golding M, Karakaya S, Kirkhus B, Le Feunteun S, Lesmes U, MacIerzanka A, MacKie A, Marze S, McClements DJ, Ménard O, Recio I, Santos CN, Singh RP, Vegarud GE, Wickham MSJ, Weitschies W, Brodkorb A (2014) A standardised static in vitro digestion method suitable for food- an international consensus. Food Funct 5:1113–1124. https://doi.org/10.1039/c3fo60702j

Mir SA, Bosco SJD, Shah MA, Santhalakshmy S, Mir MM (2017) Effect of apple pomace on quality characteristics of brown rice based cracker. J Saudi Soc Agric Sci 16:25–32. https://doi.org/10.1016/j.jssas.2015.01.001

Pasqualone A, Punzi R, Trani A, Summo C, Paradiso VM, Caponio F, Gambacorta G (2017) Enrichment of fresh pasta with antioxidant extracts obtained from artichoke canning by-products by ultrasound-assisted technology and quality characterisation of the end product. Int J Food Sci Technol 52:2078–2087. https://doi.org/10.1111/ijfs.13486

Pinto J, Spínola V, Llorent-Martínez EJ, Fernández-de Córdova ML, Molina-García L, Castilho PC (2017) Polyphenolic profile and antioxidant activities of Madeiran elderberry (*Sambucus lanceolata*) as affected by simulated in vitro digestion. Food Res Int 100:404–410. https://doi.org/10.1016/j.foodres.2017.03.044

Punzi R, Paradiso A, Fasciano C, Trani A, Faccia M, De Pinto MC, Gambacorta G (2014) Phenols and antioxidant activity *in vitro* and *in vivo* of aqueous extracts obtained by ultrasound-assisted extraction from artichoke by-products. Nat Prod Commun9:1315–1318. https://doi.org/10.1177/1934578x1400900924

Ranjha MMAN, Amjad S, Ashraf S, Khawar L, Safdar MN, Jabbar S, Nadeem M, Mahmood S, Murtaza MA (2020) Extraction of polyphenols from apple and pomegranate peels employing different extraction techniques for the development of functional date bars. Int J Fruit Sci 20:S1201–S1221. https://doi.org/10.1080/15538362.2020.1782804

Rashidinejad A, Birch EJ, Everett DW (2016) The behaviour of green tea catechins in a full-fat milk system under conditions mimicking the cheesemaking process. Int J Food Sci Nutr 67:624–631. https://doi.org/10.1080/09637486.2016.1195797

Rodrigues MJ, Neves V, Martins A, Rauter AP, Neng NR, Nogueira JMF, Varela J, Barreira L, Custódio L (2016) In vitro antioxidant and anti-inflammatory properties of Limonium algarvense flowers' infusions and decoctions: A comparison with green tea (*Camellia sinensis*). Food Chem 200:322–329. https://doi.org/10.1016/j.foodchem.2016.01.048

Stevigny C, Rolle L, Valentini N, Zeppa G (2007) Optimization of extraction of phenolic content from hazelnut shell using response surface methodology. J Sci Food Agric 87:2817–2822. https://doi.org/10.1002/jsfa

Taş NG, Gökmen V (2015) Bioactive compounds in different hazelnut varieties and their skins. J Food Compos Anal 43:203–208. https://doi.org/10.1016/j.jfca.2015.07.003

Türkmen Erol N, Sari F, Çalikoğlu E, Velioğlu YS (2009) Green and roasted mate: Phenolic profile and antioxidant activity. Turkish J Agric For 33:353–362. https://doi.org/10.3906/tar-0901-4

Vázquez G, Fernández-Agulló A, Gómez-Castro C, Freire MS, Antorrena G, González-Álvarez J (2012) Response surface optimization of antioxidants extraction from chestnut (*Castanea sativa*) bur. Ind Crops Prod 35:126–134. https://doi.org/10.1016/j.indcrop.2011.06.022

Wang S, Amigo-Benavent M, Mateos R, Bravo L, Sarriá B (2017) Effects of *in vitro* digestion and storage on the phenolic content and antioxidant capacity of a red grape pomace. Int J Food Sci Nutr 68:188–200. https://doi.org/10.1080/09637486.2016.1228099

Win MM, Abdul-Hamid A, Baharin BS, Anwar F, Sabu MC, Pak-dek MS (2011) Phenolic compounds and antioxidant activity of peanut's skin, hull, raw kernel and roasted kernel flour. Pakistan J Bot 43:1635–1642

Xiong J, Chan YH, Rathinasabapathy T, Grace MH, Komarnytsky S, Lila MA (2020) Enhanced stability of berry pomace polyphenols delivered in protein-polyphenol aggregate particles to an *in vitro* gastrointestinal digestion model. Food Chem331:127279. https://doi.org/10.1016/j.foodchem.2020.127279

Yu J, Ahmedna M, Goktepe I (2005) Effects of processing methods and extraction solvents on concentration and antioxidant activity of peanut skin phenolics. Food Chem 90:199–206. https://doi.org/10.1016/j.foodchem.2004.03.048

Zardo I, de Espíndola Sobczyk A, Marczak LDF, Sarkis J (2019) Optimization of ultrasound assisted extraction of phenolic compounds from sunflower seed cake using response surface methodology. Waste and Biomass Valorization 10:33–44. https://doi.org/10.1007/s12649-017-0038-3